AIAA-92-0439
A One-Equation Turbulence Model for Aerodynamic Flows

P. R. Spalart and S. R. Allmaras
Boeing Commercial Airplane Group
Seattle, WA 98214-2207

30th Aerospace Sciences Meeting & Exhibit
January 6-9, 1992 / Reno, NV

A ONE-EQUATION TURBULENCE MODEL FOR AERODYNAMIC FLOWS

P. R. Spalart
S. R. Allmaras*

Boeing Commercial Airplane Group
P.O. Box 3707, MS 7H-96
Seattle, WA 98124-2207

Abstract

A transport equation for the turbulent viscosity was assembled, using empiricism and arguments of dimensional analysis, Galilean invariance, and selective dependence on the molecular viscosity. It has similarities with the models of Nee & Kovasznay, Secundov *et al.*, and Baldwin & Barth. The equation includes a destruction term that depends on the distance to the wall, related to the one in Secundov's model and to one due to Hunt. Unlike early one-equation models the resulting turbulence model is local (i.e., the equation at one point does not depend on the solution at other points), and therefore compatible with grids of any structure and Navier-Stokes solvers in two or three dimensions. It is numerically forgiving, in terms of near-wall resolution and stiffness, and yields fairly rapid convergence to steady state. The wall and freestream boundary conditions are trivial. The model yields relatively smooth laminar-turbulent transition, at points specified by the user. It is powerful enough to be calibrated on 2–D mixing layers, wakes, and flat-plate boundary layers, which we consider to be the building blocks for aerodynamic flows. It yields satisfactory predictions of boundary layers in pressure gradients. Its numerical implementation in a 2-D steady-state Navier-Stokes solver has been completed and is discussed. The cases presented include shock-induced separation and a blunt trailing edge. The model locates shocks slightly farther forward than the Johnson-King model. It performs well in the near wake and appears to be a good candidate for more complex flows such as high-lift systems or wing-body junctions. However, it is not clear whether steady solutions will or should be obtained.

*Member AIAA

Motivation and Related Work

The aerodynamics community feels the need for, and is ready to invest in, a new generation of turbulence models, more onerous than the algebraic models but with a wider envelope in terms of flow and grid complexity. The Baldwin-Lomax model [1] made Navier-Stokes calculations possible in situations that are awkward for the Cebeci-Smith model [2], because the thicknesses of the boundary layer are not well defined. The Johnson-King model [3] has by-and-large fulfilled the demand for more accurate prediction of shock/boundary-layer interactions, compared with the Cebeci-Smith and Baldwin-Lomax results. However these models, even when used in Navier-Stokes codes, are boundary-layer models in spirit. Physically, they treat the whole boundary layer as a single, tightly-coupled module, which becomes incorrect when detached and multiple shear layers are present. At the implementation level, they rely on surveying the velocity or vorticity profile on a smooth grid line, roughly orthogonal to the surface, thus being "nonlocal". This becomes expensive and awkward when an unstructured grid is used [4]. Even when the only complication is that two solid bodies are present, implementing an algebraic model requires decisions that border on artificial intelligence and cannot be fully automated. This comes in addition to the poor accuracy expected when a boundary-layer model is applied to a massively-separated flow, for instance. Generalizations of algebraic models to multiple thin shear layers are quite conceivable in boundary-layer calculation methods, by combining the eddy viscosity "sustained" by each shear layer and confined to its vicinity. However, in full 2–D calculations, the orientation of the grid lines with respect to these shear layers is not under control. In addition, unstructured-grid methods are becoming more common. Finally, we do not know of an algebraic model that ensures continuity of the eddy viscosity between the airfoil block and the wake block, in a C-grid setting, while offering a plausible formula in the wake. We have abandoned efforts in that direction.

On the other hand, transport-equation models such as k-ϵ and higher models [5] are usually "local", although some have non-local near-wall terms, and have been available for years. However, they are far from having shown a decisive advantage for the prediction of shock/boundary-layer interactions or separation from smooth surfaces [6]. They may be superior for massive separation, but we do not have enough data, nor powerful enough codes, to assess that. They are also much more difficult to use. This is not so much because of the extra storage, but because they require finer grids near a wall, involve strong source terms that often degrade the convergence, and demand non-trivial upstream and freestream conditions for the turbulence variables. The near-wall problems often lead to the use of wall functions [7], which are unwieldy and lose any justification in the situation that matters most, namely, separation.

The new Baldwin-Barth model [8] is an attractive intermediate. It has only one equation and is local, except for the y^+ dependence which they plan to dispose of in the long term. It is derived from the k-ϵ model, through some further assumptions. Near the wall it does not require finer resolution than the velocity field itself. Depending on the version, it predicts adverse-pressure-gradient cases and shock interactions better than Baldwin-Lomax, but not consistently as well as Johnson-King. Its accuracy will improve in time, and it is much more practical than two-equation models. We make more specific remarks on this model during the presentation of the new one.

The present project was prompted by Baldwin & Barth's work, and by the belief that generating a one-equation model as a simplified version of the k-ϵ model is not optimal. A one-equation model is simple enough that it can be generated "from scratch", which may lead to better performance and certainly gives fuller control over its mechanics. A case in point is the Baldwin-Barth diffusion term, which is constrained by the k-ϵ ancestry and the further assumptions made. We also allow a "semi-local" near-wall term, as described below. Our calibration strategy was different. We expect to show that the new model has the same properties as that of Baldwin & Barth in terms of compatibility with unstructured grids and benign near-wall behavior, and is more accurate, especially away from the wall, as well as slightly more robust. For instance, it accepts zero values in the freestream.

The roster of one-equation models also includes those of Bradshaw, Ferriss, & Atwell [9], Nee & Kovasznay [10], Secundov and his co-workers [11], and Mitcheltree, Salas, & Hassan [12]. Except for Secundov's and Baldwin & Barth's, these models are not local, since they use length scales related to the boundary-layer thickness. This contributes to the common claim that one-equation models are not "complete" (i.e., they require a carefully-chosen length scale for each new flow) and that two-equation models are the simplest complete models. The Nee-Kovasznay model was not followed upon partly because it was not affordable at the time (1969). The Secundov model is currently entered in the Collaborative Testing of Turbulence Models (CTTM, [13]) and Prof. Bradshaw was kind enough to provide the one-page description that was submitted. Dr. Secundov provided a few details in a personal communication as well as a list of publications ranging from 1971 to 1986, but none in English. This model is presented as an evolution of the Nee-Kovasznay model but is rich in near-wall and compressibility corrections. In particular we "reinvented" their near-wall destruction term. It is expected for simple empirical models, developed under roughly the same constraints (invariance, and so on), to exhibit strong similarities. However, the leeway is large enough to produce models with widely different performance.

Presentation and Calibration of the Model

Overview

In this section we present four nested versions of the model from the simplest, applicable to free shear flows, to the most complete, applicable to viscous flows past solid bodies and with laminar regions. As each additional physical effect is considered, new terms are added and calibrated. They are identified by a common letter subscript in the constants and functions involved (e.g., constant c_{b1}, function f_{v2}; note that the constants are normalized so that the functions are of order 1). The new terms are passive in all the lower versions of the model, so that the calibration proceeds in order. This presentation may seem heavy, but should be instructive as it allows the reader to criticize the theory or the calibration layer by layer and to test the relevant version in the situation he or she chooses. It should also help preserve some clarity in later alterations of the model. The Appendix gives a compendium of the equations for the complete model.

Constitutive Relation

The central quantity is the eddy viscosity ν_t. The Reynolds stresses are given by $-\overline{u_i u_j} = 2\nu_t S_{ij}$ where $S_{ij} \equiv (\partial U_i/\partial x_j + \partial U_j/\partial x_i)/2$ is the strain-rate tensor. Compared with a two-equation model we naturally miss the k term (turbulence kinetic energy). This is not a major effect in thin shear flows, and the addition of $2k/3$ to the diagonal elements of the stress tensor is approximate in any case. Note that even in two-equation models there has been an erosion of the meaning of k itself [14], and also that the equation $\nu_t = C_\mu k^2/\epsilon$ is clearly not satisfied in the log layer with the true k and

ϵ. We are basing this criticism on experimental and direct-simulation results [15].

In a one-equation model, or in other models (e.g., zero-equation) which produce ν_t but not k, we could obtain a rough approximation of k as proportional to the stresses given by $\nu_t S_{ij}$, and introduce it on the diagonal. It would certainly be consistent to make it large enough for the Reynolds-stress tensor to be positive-definite. Usually the trace of the tensor is significantly larger than needed for positive-definiteness, with a given deviator. The eigenvalues are roughly $k/3$, $2k/3$ and k in a shear flow; none are very close to 0. We can approach this by adding $\sqrt{2}\nu_t\sqrt{S_{ij}S_{ij}}/(3a_1)$ to each diagonal element, where a_1 is the "structure parameter" [9]. This approximation may have some value in flows other than thin shear layers, even though it is far from universal. For instance, it fails on the centerline of a wake. The difficulties in introducing such a nonlinear component in the turbulent term of the momentum equation may be another factor.

Free Shear Flows

Turning our attention to ν_t itself, since there is no exact transport equation we could approximate term by term, we take an empirical approach. We do not even follow the classical procedure of establishing and calibrating the model in homogeneous turbulent flows first. This is because the model, with its single equation, is too simple to yield rich behavior in homogeneous turbulence, and also because of our emphasis on aerodynamic flows and our limited interest in homogeneous turbulence. Thus we proceed to a model equipped with diffusion terms and calibrate only at that level.

We construct the model by gathering quantities, derived from the mean flow field and from ν_t, which have Galilean invariance. For instance, the mean velocity U is not receivable. We then invoke common notions of turbulence—for instance, related to its diffusion—to assemble dimensionally correct terms that together can constitute a plausible transport equation for ν_t. We consider free shear flows at high Reynolds numbers, and accordingly the molecular viscosity is not allowed in the equation. The reasoning is that in such flows the energy and information cascades flow only from the large scales to the small scales.

The left-hand side of the equation, for correct invariance, is naturally the Lagrangian or material derivative of ν_t: $D\nu_t/Dt \equiv \partial\nu_t/\partial t + U_i\partial\nu_t/\partial x_i$. On the right-hand side we provide a production term, and diffusion terms.

For the production term, the deformation tensor $\partial U_i/\partial x_j$ presents itself. Since ν_t is a scalar we seek a scalar norm, denoted by S, of that tensor. $S\nu_t$ then has the desired dimension. A term such as $\partial V/\partial x$ (obvious notation), however tempting to mimic streamline-curvature effects, is not properly invariant. We have used the vorticity $\omega \equiv \sqrt{\Omega_{ij}\Omega_{ij}}$, where $\Omega_{ij} \equiv \partial U_i/\partial x_j - \partial U_j/\partial x_i$. The argument is that, in the flows of interest to us, turbulence is found only where vorticity is, both emanating from the solid boundaries. There are regions of vorticity without turbulence behind shocks; it is normally too weak to produce much eddy viscosity. There is a case for using the strain rate $\sqrt{2S_{ij}S_{ij}}$ or the norm of the whole tensor $\sqrt{U_{i,j}U_{i,j}}$ instead of ω, but we have not yet tested the model in cases for which it would make a difference. We normalize any candidate so that it reduces to $|U_y|$ in a simple shear flow. Note that $|U_y|$ is not a smooth quantity, but it does not seem to upset the numerical methods.

The production term, and in fact the restriction of the model to homogeneous turbulence, is

$$\frac{D\nu_t}{Dt} = c_{b1}\, S\, \nu_t. \qquad (1)$$

The subscript b stands for "basic". The response of the model in homogeneous turbulence is dull, but not grossly inaccurate. The eddy viscosity is stationary in isotropic turbulence ($D\nu_t/Dt = 0$, because $S = 0$). It is accepted that in such a flow the energy k is proportional to $t^{-6/5}$. Then the simplest combination that has the same dimensions as ν_t, namely k^2/ϵ where ϵ is the dissipation, slowly decays like $t^{-1/5}$. In anisotropic flows ν_t can only increase under the effect of production, in a manner that depends on the choice of S. That choice may be re-examined later, but if we consider a shear flow with $S \equiv |U_y|$ we observe that ν_t grows exponentially like $\exp(c_{b1}St)$. This is the "classical" behavior for shear flow, with a growth rate in the 0.1 to 0.16 range according to experiments. Our calibration on inhomogeneous flows yields values of c_{b1} between 0.13 and 0.14. Thus, we do not emphasize homogeneous turbulence, but we are not in strong conflict with it. The Baldwin-Barth and Secundov models have rather large production constants, at least 0.2. Note that we have not found any plausible and invariant quantity that could constitute a destruction term away from walls. We return to this issue later.

The search for diffusion terms naturally focuses on spatial derivatives of ν_t. Classical diffusion operators are of the type $\nabla.([\nu_t/\sigma]\nabla\nu_t)$ with σ a turbulent Prandtl number. They conserve the integral of ν_t, save for boundary contributions. However there is no reason why the integral of ν_t should be conserved. Manipulations of two-equation models often bring out diffusion terms that are not conservative, for instance cross-terms between ∇k and $\nabla\epsilon$. By analogy we allow a non-conservative diffusion term, involving first derivatives of ν_t. We arrive at the following "basic" model:

$$\frac{D\nu_t}{Dt} = c_{b1}\, S\, \nu_t + \frac{1}{\sigma}\left[\nabla.(\nu_t\nabla\nu_t) + c_{b2}\,(\nabla\nu_t)^2\right]. \qquad (2)$$

We break our convention for σ, which belongs to the c_b series, because of the traditional notation of Prandtl numbers.

The diffusion term of (2) conserves the integral of the quantity $\nu_t^{1+c_{b2}}$. Recall the lack of a destruction term. This lack was responsible for a mild inconsistency in isotropic turbulence. It could also invalidate the model in the class of shear flows in which ν_t decreases (negative $D\nu_t/Dt$) such as an axisymmetric wake. However, the diffusion term can easily bring down the centerline value of ν_t, and the true constraint is that under (2) the integral of $\nu_t^{1+c_{b2}}$ cannot decrease. With the classical exponents of the self-similar axisymmetric wake (length scale $\propto t^{1/3}$, velocity $\propto t^{-2/3}$), we find that the integral increases provided that $c_{b2} \leq 1$. Even if the calibration does not include the axisymmetric wake, it is preferable to satisfy this constraint.

Another constraint may be obtained from the behavior of a turbulent front. The diffusion term admits the following (weak) one-dimensional solution:

$$\nu_t(x,t) = \max\left(0, \quad A\left[x + \frac{A(1+c_{b2})}{\sigma}\, t\right]\right), \qquad (3)$$

for any constant A. This is a linear ramp propagating at the velocity $-A(1+c_{b2})/\sigma$. If $c_{b2} > -1$ it propagates into the non-turbulent region, which is physically correct. The equivalent of c_{b2} is 0 in the Secundov model (the diffusion term is conservative). It equaled -2 in the original Baldwin-Barth model [16] and is somewhat below -1 in the published version [8], so that under the diffusion term alone the turbulent front recedes. We believe this effect is to blame for the sensitivity of that model to the freestream value of ν_t (or R_T). Note that Baldwin & Barth are constrained in their choice of c_{b2} by the connection with the k-ϵ model, in the original version, and by their calibration in the log layer, in all versions. We avoid this constraint thanks to a near-wall term as explained below. The weak solution shown in (3) is of great interest in practice, as it indeed gives the structure of the solution at the edge of a turbulent region. This occurs because the diffusion term dominates there (see Fig. 6, below).

An approximate analysis of the turbulent front, coupling the eddy viscosity and the shear rate, indicates that the ratio $(1+c_{b2})/\sigma$ also deserves attention. If it is larger than 2 the eddy-viscosity front, which is a ramp, is slightly ahead of the shear front, making the velocity profile smoother. If it is lower than 2 the two fronts coincide. If it equals 1 the velocity profile of a mixing layer is exactly triangular, i.e., $|U_y|$ exhibits a step which is unphysical. Although these considerations border on the cosmetic they indicate that $(1+c_{b2})/\sigma$ should be larger than 1 and suggest that 2 may be a favorable value.

The fact that the dependent variable ν_t itself is the diffusion coefficient is responsible for the existence of weak solutions such as (3), and raises the possibility of non-unique solutions. Indeed if the initial condition is $|x|$, we have a weak solution in which ν_t behaves like $|x|^{1/(2+c_{b2})}$ near $x = 0$, and a smooth solution with $\nu_t > 0$ at $x = 0$. The difference is confined to a boundary layer near $x = 0$. In a numerical setting with straightforward second-order centered differencing, the weak solution will be obtained if the diffusion term is written $\nu_t\nabla^2\nu_t + (1+c_{b2})(\nabla\nu_t)^2$, but the smooth solution will be obtained if it is written as in (2). Other forms that give the smooth solution are $\nabla^2(\nu_t^2/2) + c_{b2}(\nabla\nu_t)^2$ and $(1+c_{b2})\nabla(\nu_t\nabla\nu_t) - c_{b2}\nu_t\nabla^2\nu_t$. The later addition of a term proportional to the molecular viscosity formally resolves this non-uniqueness and leads to the smooth solution with $\nu_t > 0$. However, particularly at high Reynolds numbers, it is desirable to use a favorable form of the diffusion term.

Outside a turbulent shear flow the Reynolds stresses, particularly the diagonal components, do not exactly vanish. However, they are induced by pressure fluctuations and bear little relationship to the local strain tensor S_{ij}. For that reason, it is as well to have the eddy viscosity be zero outside the turbulent region, and this is the value we recommend in the freestream. In addition, the model is essentially insensitive to non-zero values (which may help some numerical solvers), provided that they are much smaller than the values in the turbulent region. This is due to the dominance of the turbulent region ($\nu_t > 0$) over the non-turbulent one, as illustrated by the ramp solution (3). This feature adds to the "black box" character of the new model and represents a substantial advantage over the Baldwin-Barth model and many two-equation models, some of which are highly sensitive to freestream values—that of the time scale for instance.

The amplification of the eddy viscosity by the production term is of interest. Note that the linearization of (2) for small ν_t preserves only the production term. Consider the steady flow at a velocity U_∞ past a body of size L, with thin shear- or boundary layers of thickness δ; these are orders of magnitude. Outside the thin shear layers the deformation tensor is of order U_∞/L so that, irrespective of the exact definition of S, the logarithm of the amplification ratio will be on the order of c_{b1} (a growth rate on the order of $c_{b1}S$ over a residence time on the order of L/U_∞). Thus, small values will remain small. In contrast in the thin shear layers the logarithm of the amplification ratio under the effect of the production term alone would be on the order of $c_{b1}L/\delta$, and therefore large in the usual situation since $L \gg \delta$. Thus small values of ν_t, whether inherited from the freestream, or resulting from numerical errors, or introduced intentionally at the "trip" as described later, will cause transition in the thin shear layers only. By transition we mean growth to such levels that the diffusion terms, which are nonlinear, become active. The

destruction term introduced later is also nonlinear. The sequence of exponential growth, followed by saturation at levels on the order of $U_\infty \delta$, is consistently observed in practice. Note also that even though the contribution of the c_{b2} term is positive the diffusion terms cannot cause runaway growth. This is so because their contribution is negative at a local maximum of ν_t. Recall also the constraint on the integral of $\nu_t^{1+c_{b2}}$. The eddy-viscosity budget in a well-developed solution always includes a sizeable contribution from the production term.

We now calibrate the free-shear-flow version of the model by requiring correct levels of shear stress in two-dimensional mixing layers and wakes. Fair values for the peak shear stress are $0.01(\Delta U)^2$ in the mixing layer and $0.06(\Delta U)^2$ in the wake, where ΔU is the peak velocity difference [17]. This gives two conditions for three free constants c_{b1}, σ, and c_{b2}, and leaves a one-dimensional family of "solutions" which is shown in Fig. 1 parametrized by the Prandtl number σ, the easiest quantity to interpret. The range of values of σ we consider plausible is at most $[0.6, 1]$. The corresponding values of c_{b2} are between 0.6 and 0.7 and satisfy our "guidelines" ($-1 < c_{b2} \leq 1$) with a margin. The ratio $(1+c_{b2})/\sigma$ varies from about 2.7 to 1.7 and also satisfies its guideline (> 1).

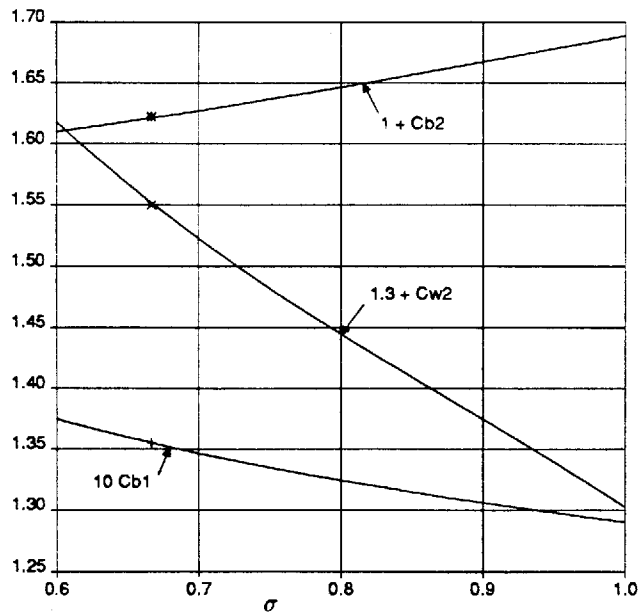

Figure 1: Calibrated model constants. — locus of solutions; +, ×, * point selected for the calculations.

The solutions were obtained numerically using a stretched grid, centered second-order finite differences, Runge-Kutta fourth-order time integration, and zero values in the freestream. This artless treatment would rapidly reveal poor numerical properties in the model. The growth of the layers was followed until a self-similar state was attained. The solutions exhibit the ramp structure at the edge of the turbulent region, as seen in the mixing-layer case in Fig. 2. The centered-difference solution cannot faithfully reproduce a weak solution at the front, but the disturbance does not propagate. Time steps in excess of the stability limit were revealed first by short oscillations near the centerline.

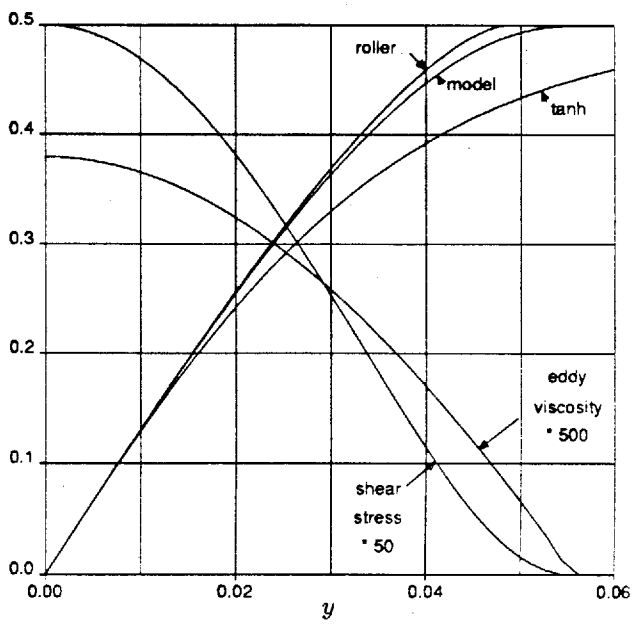

Figure 2: Profiles in a time-developing mixing layer. Normalized with velocity difference and time. Velocity profiles adjusted to the same slope at $y = 0$.

Based primarily on the edge behavior, we favor a fairly diffusive member of our "plausible" range, namely $\sigma = 2/3$, $c_{b1} = 0.1355$, $c_{b2} = 0.622$, $(1+c_{b2})/\sigma \approx 2.4$. In the mixing layer it gives a velocity profile close to that associated with identical "rollers" of uniform vorticity (see Fig. 2). Very low values of σ would be needed to bring it close to the hyperbolic-tangent profile, which is a common approximation. In the wake the peak eddy viscosity is $0.46M$ where M is the momentum of the wake, in good agreement with experiment [18]. We did not attempt to match any axisymmetric flow, partly because they are not prevalent in our applications and partly because, for most models, these flows conflict with the 2-D flows. The model is not intended to be universal.

Near-wall Region, high Reynolds Number

In a boundary layer the blocking effect of a wall is felt at a distance through the pressure term, which acts as the main destruction term for the Reynolds shear stress. This suggests a destruction term in the transport equation for the eddy viscosity. Dimensional analysis leads to a combination $-c_{w1}(\nu_t/d)^2$, with d the distance to the wall. The subscript w stands for "wall". This

term will be passive in free shear flows ($d \to \infty$) and therefore does not interfere with our calibration up to this point. The Secundov model includes this type of term (however their term differs from ours in the viscous and the outer regions). The idea of a near-wall, but not viscous, "blocking" term is also in Hunt [19]. It is also related to the algebraic models, which take the smaller of two eddy viscosities. The outer eddy viscosity scales with the boundary-layer thickness, and the inner eddy viscosity is given by the mixing length, $l \propto d$.

In a classical log layer with friction velocity u_τ we have $S = u_\tau/(\kappa d)$ and $\nu_t = u_\tau \kappa d$. Equilibrium between the production and diffusion terms (all positive) and the destruction term is possible provided
$c_{w1} = c_{b1}/\kappa^2 + (1 + c_{b2})/\sigma$.

Tests show that the model, when equipped with the destruction term, can produce an accurate log layer. This relies on the treatment of the viscous region, described below. On the other hand it produces too low a skin-friction coefficient in a flat-plate boundary layer. This shows that the destruction term as formulated decays too slowly in the outer region of the boundary layer. To address this deficiency and allow a new calibration we multiply it by a non-dimensional function f_w, which equals 1 in the log layer. Note that c_{w1} is not negotiable (i.e., we would not adjust the C_f at the expense of the log-law constants), and also that we were not able to obtain an accurate skin friction just by using the freedom left by the free-shear-flow calibration (Fig. 1). The model becomes

$$\frac{D\nu_t}{Dt} = c_{b1} S \nu_t + \frac{1}{\sigma}\left[\nabla\cdot(\nu_t \nabla \nu_t) + c_{b2}(\nabla \nu_t)^2\right] - c_{w1} f_w \left[\frac{\nu_t}{d}\right]^2 \quad (4)$$

Note that Secundov *et al.* did not follow the f_w route.

The choice of an adequate argument for f_w was inspired by algebraic models, in which the mixing length plays a major role near the wall. This length can be defined by $l \equiv \sqrt{\nu_t/S}$ and we use the square of $l/\kappa d$ as a convenient non-dimensional argument:

$$r \equiv \frac{\nu_t}{S\kappa^2 d^2}. \quad (5)$$

Both r and f_w equal 1 in the log layer, and decrease in the outer region. Note that any dimensionally correct function of (ν_t, d, S) that reduces to $-c_{w1}\kappa^2 u_\tau^2$ in a log layer would be as eligible as the one we are choosing (4). A satisfactory f_w function is

$$f_w(r) = g\left[\frac{1 + c_{w3}^6}{g^6 + c_{w3}^6}\right]^{1/6}, \qquad g = r + c_{w2}(r^6 - r). \quad (6)$$

This function is shown in Fig. 3. The results are most sensitive to the slope of f_w at $r = 1$, which is controlled by c_{w2}. The step from g to f_w is merely a limiter that prevents large values of f_w, which could upset the code and give an undeserved importance to the

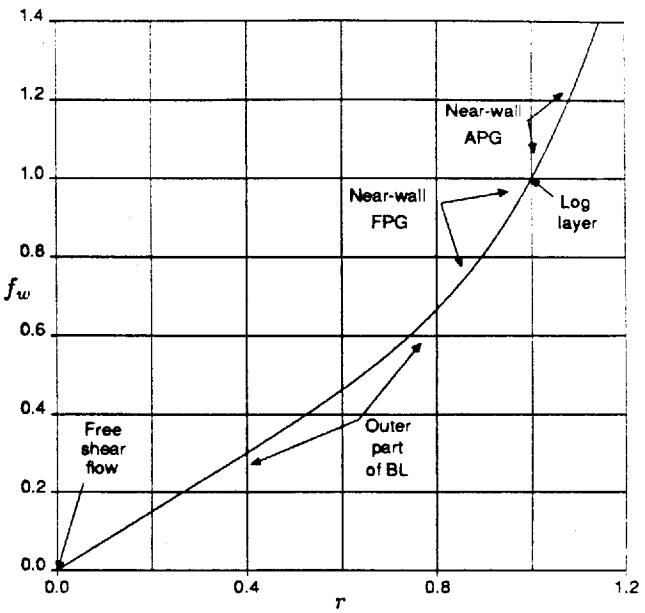

Figure 3: f_w function involved in the destruction term, see (4-6).

fact that S may vanish. The region $r > 1$ is exercised only in adverse pressure gradients, and then rarely beyond $r = 1.1$. Having $f_w(0) = 0$ is not essential, because in free shear flows the destruction term vanishes on account of the d^2 in its denominator. A reasonable value for c_{w3} is 2. We then calibrate c_{w2} to match the skin-friction coefficient in a flat-plate boundary layer. We adopt the value of the CTTM, namely $C_f = 0.00262$ at $R_\theta = 10^4$ [13], which requires $c_{w2} = 0.3$. All the boundary-layer tests relied on a code written by Mr. D. Darmofal, of M.I.T., during a short stay at Boeing.

Figure 4 shows the velocity, eddy-viscosity, and shear-stress profiles in a flat plate boundary layer at $R_\theta \approx 10^4$. At 10^4, $C_f = 0.00262$ and $H = 1.31$. The Clauser shape factor $G \equiv \sqrt{2/C_f}(H-1)/H$ is settled at 6.6. and the shape of the profile is satisfactory. Notice again the ramp structure of ν_t at the edge of the shear flow. The peak value of ν_t is $0.021 U_\infty \delta^*$, compared with $0.0168 U_\infty \delta^*$ in the Cebeci-Smith model [2]. Conversely, the Cebeci-Smith eddy viscosity is higher near $y/\delta^* = 1$. The shear-stress profile approaches the wall with a finite slope, rapidly turning to zero slope at the wall as discussed in the context of direct-simulation results [15].

Figure 5 shows the velocity profile in wall coordinates, illustrating the log layer and the smooth departure in the wake. Again, the shape of the outer region appears good, showing that the destruction term and the f_w function are fair approximations, at least in this flow. The arrival at the freestream velocity is a little too abrupt, as it was in the mixing layer, in Fig. 2. This behavior cannot be corrected except by making the model very diffusive (low σ).

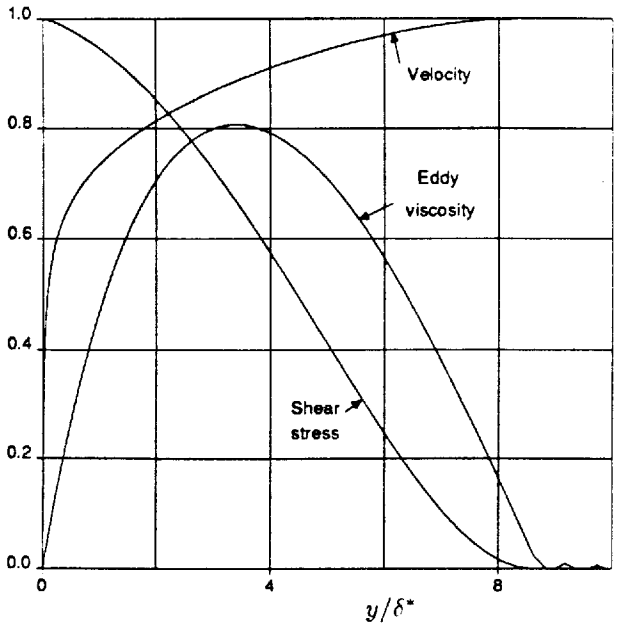

Figure 4: Profiles in a flat-plate boundary layer at $R_\theta \approx 10^4$, outer coordinates. U normalized with U_∞, τ with τ_{wall}, and ν_t with $0.025 U_\infty \delta^*$.

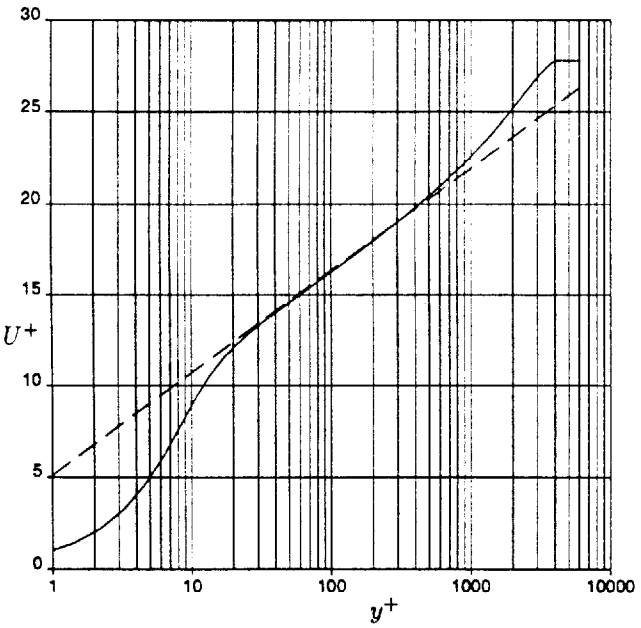

Figure 5: Velocity profile in a flat-plate boundary layer at $R_\theta \approx 10^4$, inner coordinates. — model; - - - log law.

The budget of ν_t is shown in Fig. 6. The sum (i.e., $D\nu_t/Dt$) is positive throughout. It is 0 at the wall, then roughly follows a ramp up to the edge of the turbulent region. Its outer part is representative of the outer part of either one of the free shear flows, including the vanishing contribution of the destruction term. The production is equal to the shear stress. In the outer part the diffusion is primarily responsible for the advance of the turbulent front, in qualitative agreement with the budgets of "legitimate" turbulence quantities such as the kinetic energy. Near the wall the diffusion again makes a strong positive contribution, balanced by the destruction. The ideal near-wall budget is, in the units of the figure, production $= 1$, diffusion $= \kappa^2(1+c_{b2})/\sigma/c_{b1} \approx 3$, destruction $= -1-\kappa^2(1+c_{b2})/\sigma/c_{b1} \approx -4$. Note that it is not maintained far up into the layer at all; correspondingly, ν_t does not follow its ideal linear log-layer behavior ($\kappa y u_\tau$) far up either (see Fig. 4). However this does not prevent a log layer from forming.

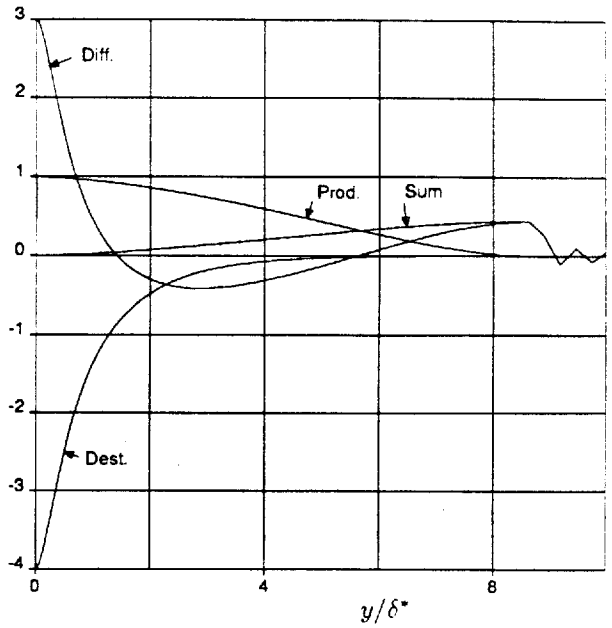

Figure 6: Eddy-viscosity budget in a flat-plate boundary layer. Normalized with τ_{wall}.

This completes the calibration of the model save for viscous effects. We later examine the performance of the model in what is probably the most sensitive situation, the outer region of a boundary layer in adverse pressure gradient.

Near-wall Region, finite Reynolds Number

In the buffer layer and viscous sublayer, additional notation is needed. Besides the wall units, y^+ and so on, we introduce $\tilde{\nu}$ which will equal ν_t except in the viscous region, and $\chi \equiv \tilde{\nu}/\nu$. This is in analogy with Mellor & Herring's notation [20], because from the wall to the log layer we have $\chi = \kappa y^+$.

We follow Baldwin & Barth [8] in choosing a transported quantity $\tilde{\nu}$ which behaves linearly near the wall. This is beneficial for numerical solutions: $\tilde{\nu}$ is actually easier to resolve than U itself, in contrast with ϵ, for instance. Therefore, the model will not require a finer grid than an algebraic model would. To arrive at this

we consider the classical log layer and devise near-wall "damping functions" that are compatible with known results. These functions are distinct from the f_w near-wall inviscid destruction term.

The eddy viscosity ν_t equals $\kappa y u_\tau$ in the log layer, but not in the buffer layer. We define $\tilde{\nu}$ so that it equals $\kappa y u_\tau$ all the way to the wall. This leads to

$$\nu_t = \tilde{\nu}\, f_{v1}, \qquad f_{v1} = \frac{\chi^3}{\chi^3 + c_{v1}^3}. \tag{7}$$

The f_{v1} function is borrowed from Mellor & Herring. The subscript v stands for "viscous". We prefer the value $c_{v1} = 7.1$ to Mellor & Herring's 6.9, which we believe yields a low intercept for the log law. Other f_{v1} functions could be used, for instance the one compatible with the Van-Driest damping is $f_{v1} = (\sqrt{1+4l^{+2}} - 1)/2\chi$, where $l^+ = \chi[1 - \exp(-\chi/\kappa A^+)]$ and A^+ is the familiar 26 [2]. We have not encountered cases for which the choice of f_{v1} made a difference. Note that there is no basis for (7) to apply at the edge of the turbulent region, where χ is also of order 1 and smaller. However, the eddy viscosity has little influence there, because of the absence of steep gradients.

The production term also needs attention. In it S is replaced with $\tilde{S}$, given by

$$\tilde{S} \equiv S + \frac{\tilde{\nu}}{\kappa^2 d^2} f_{v2}, \qquad f_{v2} = 1 - \frac{\chi}{1 + \chi f_{v1}}. \tag{8}$$

The function f_{v2} is constructed, just like f_{v1}, so that $\tilde{S}$ would maintain its log-layer behavior ($\tilde{S} = u_\tau/(\kappa y)$) all the way to the wall. $\tilde{S}$ is singular at the wall, but $\tilde{\nu}$ is 0 there, so that the production is well-behaved. Note that there is a range of χ in which $\tilde{S}$ is less than S and may become negative. This should not upset the numerical solvers. Other quantities involved in the "inviscid" model are redefined in terms of $\tilde{\nu}$ instead of ν_t, for instance $r \equiv \tilde{\nu}/(\tilde{S}\kappa^2 d^2)$.

We finally add a viscous diffusion term, consistent with a Dirichlet boundary condition at the wall, $\tilde{\nu} = 0$. This term too is based on an analogy, rather than a rigorous equation. In addition $\tilde{\nu}$ behaves linearly, so that its Laplacian will be small in an established solution. Accordingly, we insert the molecular viscosity in a convenient place and pay little attention to a factor of σ. The transport equation has become

$$\frac{D\tilde{\nu}}{Dt} = c_{b1}\tilde{S}\tilde{\nu} + \frac{1}{\sigma}\left[\nabla.((\nu+\tilde{\nu})\nabla\tilde{\nu}) + c_{b2}(\nabla\tilde{\nu})^2\right] - c_{w1} f_w \left[\frac{\tilde{\nu}}{d}\right]^2 \tag{9}$$

This equation now yields equilibrium ($D\tilde{\nu}/Dt = 0$) all the way to $d = 0$ in a classical law-of-the-wall situation. Furthermore, the numerical evidence shows that this classical solution is a stable solution of the system made of the momentum equation and (9), as it has been obtained starting with a wide range of initial conditions. This includes the results of Figs. 4 and 5; in particular Fig. 5 displays the viscous and buffer layers.

Fine effects of pressure gradients or transpiration are likely to strain the accuracy of the model, although we expect the trends to be correct and the database is far from definitive. Note that the traditional tools for inserting these effects into the algebraic models are ruled out, because they are not local.

Laminar Region and Tripping

The final set of terms provides control over the laminar regions of the shear layers, a control which has two aspects: keeping the flow laminar where desired, and obtaining transition where desired. Navier-Stokes codes with algebraic models usually have crude "off-on" devices or short ramps based on the grid index along the wall. These do not help the convergence of the codes. In addition we require a device that is useable on unstructured grids. The subscript t will stand for "trip". We use this word to mean that the transition point is imposed by an actual trip, or natural but obtained from a separate method. *On no account should the turbulence model be trusted to predict the transition location.* This is true of all the models we know. Some models, including k-ϵ, predict relaminarization. In situations that should induce relaminarization, this one tends to drop the eddy viscosity to low levels, but without "snapping" to 0. We may be able to improve on this using the f_{t2} function below.

We described how transition was expected only in thin shear layers. The linearized version of (9) for small $\tilde{\nu}$ only contains the production term: $D\tilde{\nu}/Dt = c_{b1}S\tilde{\nu}$; therefore, $\tilde{\nu} = 0$ is an unstable solution of (9) (going in the direction of D/Dt). In a boundary-layer code the zero solution is easily maintained, but in a Navier-Stokes code exactly-zero values are rarely preserved, so that the model is "primed" by numerical errors upstream of the trip. It then transitions at a rate that depends on numerical details and has little to do with the boundary layer's true propensity to transition, as controlled by pressure gradient, suction, and so on. We verified this behavior, and it is not acceptable.

A solution is to alter the production term so that $\tilde{\nu} = 0$ is a stable solution, albeit with a small basin of attraction. For this we take the convention that in the laminar region $\tilde{\nu}$ is of order ν at most, and recall the argument χ. Note that if $\tilde{\nu} \leq \nu$, then $\nu_t \ll \nu$, because of the damping by f_{v1}. We multiply the production term by $1 - f_{t2}$, where

$$f_{t2} = c_{t3}\, \exp(-c_{t4}\, \chi^2). \tag{10}$$

In order for 0 to attract $\tilde{\nu}$ down from values on the order of $\nu/5$, the following values are fair: $c_{t3} = 1.1$,

$c_{t4} = 2$. In any case c_{t3} must be larger than 1. As for c_{t4} it could be decreased several-fold, if a code still yielded premature transition. The cross-over point of $1 - f_{t2}$, (i.e., the bound of the basin of attraction), is at $\chi = \sqrt{\log(c_{t3})/c_{t4}}$. However, 2 was small enough in our code. Values much smaller than 1 would start affecting the results in the turbulent region.

In order to still balance the budget near the wall we offset the change in the production term with an opposite change in the destruction term, involving f_{t2}. Again we take an empirical approach, and have numerical evidence that it yields a stable system. A user that is doing boundary-layer calculations can leave the f_{t2} term out (i.e., set $c_{t3} = 0$).

The task is now to obtain transition. We refer to transition points, in 2–D, and transition lines, in 3D. We address only boundary-layer transition, but a generalization to free shear flows will be easy. Usually each 2–D body has two transition points. We wish to initiate transition near these points in a smooth manner, and compatible with any grid. For this a source term is added that will be nonzero only in a small domain of influence. This domain should not extend outside the boundary layer. Not wanting to find this edge, nor violate invariance principles, we invoke the quantities ΔU and ω_t. ΔU is the norm of the difference between the velocity at the trip (i.e., usually zero since the wall is not moving) and that at the field point we are considering. ω_t is the vorticity at the wall at the trip point. Upstream of the trip in a boundary-layer code, it is fair to take ω at the wall at the current station, since ω at the trip is not available yet. The thickness of the boundary layer is on the order of U_e/ω_t, where U_e is the edge velocity. Recall that it is still laminar. We also introduce d_t, the distance from the field point to the trip point or line.

Storing, or repeatedly computing, d_t for each field point is a penalty, but it would not be difficult to keep a list of the points that are within a reasonable distance of the trip and to compute the trip term only for those. The user may also watch for the following peculiar situation: the body could be so thin that the trip on one side causes transition on the other side. A definition of d_t as the length of the shortest line that links the field point to the trip while not crossing the body would solve the problem, but in an expensive manner. It is simpler just to override d_t (i.e., set it to a large value) for field points and trips that are known to be on opposite sides of the body. The angle between the line from the trip to the field point and the normal to the wall may be useful.

Dimensional analysis points to ΔU^2 as a proper scale for the source term, and we arrive at

$$\frac{D\tilde{\nu}}{Dt} = c_{b1}\,[1 - f_{t2}]\;\tilde{S}\,\tilde{\nu} + \frac{1}{\sigma}\left[\nabla\cdot((\nu+\tilde{\nu})\nabla\tilde{\nu}) + c_{b2}\,(\nabla\tilde{\nu})^2\right] - \left[c_{w1} f_w - \frac{c_{b1}}{\kappa^2} f_{t2}\right]\left[\frac{\tilde{\nu}}{d}\right]^2 + f_{t1}\;\Delta U^2, \qquad (11)$$

with

$$f_{t1} = c_{t1}\;g_t\;\exp\left(-c_{t2}\;\frac{\omega_t^2}{\Delta U^2}\left[d^2 + g_t^2 d_t^2\right]\right), \qquad (12)$$

and $g_t \equiv \min(0.1, \Delta U/\omega_t \Delta x)$ where Δx is the grid spacing along the wall at the trip. This equation specifies the two f_t terms, and the trip term is the last in (11). The Gaussian in f_{t1} confines the domain of influence of the trip terms as needed; it is roughly a semi-ellipse. The magnitude is adjusted so that the integrated contribution for a particle crossing the domain of influence is on the order or $U_e\delta$, δ the boundary-layer thickness, as is ensured by typical algebraic models [2]. The odd factor g_t is passive in a situation with an extremely fine grid, but is quite active and necessary in practice. This is because the domain of influence of the trip scales with the boundary layer thickness, which is very small in the laminar part. As a result, that domain easily falls between two streamwise grid points, so that the trip is not felt at all. The g_t factor guarantees that the trip term will be nonzero over a few streamwise stations.

The value $c_{t2} = 2$ reflects typical values of $\delta\omega_t/U_e$ in laminar boundary layers and is not a candidate for much adjustment. Tests indicate a range of at least two decades for c_{t1} between values so low that transition miscarries, and values so high that $\tilde{\nu}$ and the skin-friction overshoot. The value $c_{t1} = 1$ is well within that range; successful transition was obtained with 0.1 and with 10. It is possible that at very low Reynolds numbers c_{t1} would require more attention. In any case, we recommend that the user check for transition on both surfaces. To start with, the two trips should bracket the stagnation point. Except at very low Reynolds numbers the skin-friction coefficient is enough of a criterion. Note that the trips are often near the leading edge, in a region where the skin friction has violent variations due to the pressure gradients. Therefore, it is advisable to check the skin-friction coefficient a little downstream, in a weak pressure gradient.

Note that the growth of $\tilde{\nu}$ to nonlinear levels under the effect of the production term occurs in a few boundary-layer thicknesses (c_{b1} being roughly 0.13). This is consistent with the idea that the trip term mimics the secondary instabilities invoked by recent transition theories, which have growth rates on the order of $1/\delta$. However since the streamwise grid is often much coarser than δ, transition will still appear very steep to that grid. The contribution of the trip source term is rapidly overwhelmed by the exponential amplification due to production. Thus, we have a formal advantage

over the "off-on" models in that transition is a smooth process, but in practice it is debatable. Naturally, an adaptive grid will focus points at transition, and approach the ideal situation.

Initial and Freestream Conditions

Fair results have been obtained by initially setting $\tilde{\nu}$ uniformly to its freestream value. The turbulent viscosity emanates at the trips and spreads without noticeably degrading the convergence of the code. In the freestream the ideal value is zero. Some solvers may have trouble with this, either because of round-off errors or some convergence tests dividing by $\tilde{\nu}$. Freestream values of $\tilde{\nu}$ up to roughly $\nu/10$ are easily tolerable with the current c_{t3} and c_{t4} constants. Recall that the f_{v1} factor in (7) then makes ν_t much smaller than ν, so that the laminar boundary layers are not disturbed.

Numerical Solution Procedure

We expand on the approach of Baldwin & Barth [8] for solution of the turbulence transport model within a Navier-Stokes solver. The model is advanced in time using an implicit solution procedure designed to achieve a positive turbulence field for all transient solution states, as well as a fast convergence rate to steady-state. We have incorporated the turbulence-model solution module into a modified version of Martinelli & Jameson's FLO103 [21], where the updates of the velocity field and the turbulence are decoupled at each time step. The turbulence is updated at the start of each multistage Runge-Kutta time step on the finest grid of the multigrid cycle; on coarser grids the turbulence is frozen.

We begin by rewriting the one-equation model (11) in a form more convenient for numerical analysis,

$$\frac{\partial \tilde{\nu}}{\partial t} = M(\tilde{\nu})\tilde{\nu} + P(\tilde{\nu})\tilde{\nu} - D(\tilde{\nu})\tilde{\nu} + T \qquad (13)$$

where $M(\tilde{\nu})\tilde{\nu}$ is the combined advection/diffusion terms,

$$M(\tilde{\nu})\tilde{\nu} = -(\vec{U}\cdot\nabla)\tilde{\nu} + \frac{1}{\sigma}\left[\nabla\cdot[(\nu+\tilde{\nu})\nabla\tilde{\nu}] + c_{b2}(\nabla\tilde{\nu})^2\right], \qquad (14)$$

the production source term is

$$P(\tilde{\nu})\tilde{\nu} = c_{b1}[1 - f_{t2}]\tilde{S}\tilde{\nu}, \qquad (15)$$

the wall destruction source term is

$$D(\tilde{\nu})\tilde{\nu} = \left[c_{w1}f_w - \frac{c_{b1}}{\kappa^2}f_{t2}\right]\left[\frac{\tilde{\nu}}{d}\right]^2, \qquad (16)$$

and the trip function is

$$T = f_{t1}\Delta U^2. \qquad (17)$$

Note that T and $D(\tilde{\nu})$ are always positive or zero, and $P(\tilde{\nu})$ is positive as long as $\tilde{S}$ is positive.

Care should be used in interpreting our notation. For example, the complete production operator is $P(\tilde{\nu})\tilde{\nu}$ rather than $P(\tilde{\nu})$ alone. The notation is intended to simplify the following matrix theory analysis.

The turbulence transport equation is discretized on a grid with $\mathbf{v}$ the vector of unknowns at all grid points. The solution is integrated in time using an implicit backward-Euler scheme of the form,

$$\left[\mathbf{I} - \Delta t\left(\overline{\mathbf{M}}(\mathbf{v}^n) + \overline{\mathbf{P}}(\mathbf{v}^n) - \overline{\mathbf{D}}(\mathbf{v}^n)\right)\right]\Delta\mathbf{v}^n = \Delta t\left[\mathbf{M}(\mathbf{v}^n) + \mathbf{P}(\mathbf{v}^n) - \mathbf{D}(\mathbf{v}^n)\right]\mathbf{v}^n + \Delta t\mathbf{T} \qquad (18)$$

where the nonlinear matrix operators $\mathbf{M}$, $\mathbf{P}$, $\mathbf{D}$ and $\mathbf{T}$ are the discrete analogues of M, P, D and T, respectively; $\overline{\mathbf{M}}$, $\overline{\mathbf{P}}$, $\overline{\mathbf{D}}$ are implicit matrices; Δt is the time step; and $\Delta\mathbf{v}$ is the solution change,

$$\Delta\mathbf{v}^n \equiv \mathbf{v}^{n+1} - \mathbf{v}^n. \qquad (19)$$

The exact solution of the turbulence transport equation cannot become negative. It can be shown that if $\tilde{\nu} = 0$ at some location and the surrounding values are non-negative, then $\partial\tilde{\nu}/\partial t \geq 0$. An underlying goal of the solver is to reproduce this analytic behavior—a non-negative turbulence field—throughout the solution process (i.e. $\tilde{\nu} \geq 0$ at all grid points and at all time steps).

We achieve this goal of a non-negative turbulence field through the use of positive discrete operators and M-type matrices. A positive operator, when applied to a vector of non-negative elements, will produce a vector with non-negative elements. An M-type matrix is diagonally dominant with positive diagonal elements and negative (or zero) off-diagonal elements. A key property of an M-type matrix is that its inverse contains only non-negative elements; hence, the inverse of an M-type matrix is a positive operator. Our goal can be accomplished by careful discretization and construction of the implicit operators $\overline{\mathbf{M}}$, $\overline{\mathbf{P}}$ and $\overline{\mathbf{D}}$.

Rearrangement of (18) gives $\mathbf{v}^{n+1}$ directly as a function of $\mathbf{v}^n$,

$$\left[\mathbf{I} - \Delta t\left(\overline{\mathbf{M}} + \overline{\mathbf{P}} - \overline{\mathbf{D}}\right)\right]\mathbf{v}^{n+1} = \left[\mathbf{I} + \Delta t\left((\mathbf{M} - \overline{\mathbf{M}}) + (\mathbf{P} - \overline{\mathbf{P}}) - (\mathbf{D} - \overline{\mathbf{D}})\right)\right]\mathbf{v}^n + \Delta t\mathbf{T}. \qquad (20)$$

Assuming $\mathbf{v}^n$ is non-negative, then non-negativity of $\mathbf{v}^{n+1}$ is guaranteed if the right-hand-side operator is positive and the left-hand-side operator forms an M-type matrix. Thus, sufficient constraints on the discrete operators are given by,

$$-\overline{\mathbf{M}} \quad \text{is M-type} \qquad (21a)$$

$$-\overline{\mathbf{P}} \quad \text{is M-type} \qquad (21b)$$

$$+\overline{\mathbf{D}} \quad \text{is M-type} \qquad (21c)$$

$$[\mathbf{M}-\overline{\mathbf{M}}]\,\mathbf{v}\geq 0 \qquad \text{for all } \mathbf{v}\geq 0 \qquad (22a)$$

$$[\mathbf{P}-\overline{\mathbf{P}}]\,\mathbf{v}\geq 0 \qquad \text{for all } \mathbf{v}\geq 0 \qquad (22b)$$

$$[\mathbf{D}-\overline{\mathbf{D}}]\,\mathbf{v}\leq 0 \qquad \text{for all } \mathbf{v}\geq 0 \qquad (22c)$$

Baldwin & Barth show, for their model, that similar constraints on the implicit and explicit operators in the backward-Euler scheme guarantee positivity of the discrete solution. They also show that these constraints give unconditional stability of the numerical solution procedure.

Description of the discretization and construction of implicit matrices will be given in detail for 1-D, where the notation is simpler. Extension to 2-D and 3-D is straightforward because there are no cross derivatives in the one-equation model.

The model is discretized using a cell-centered finite-difference scheme.

Advection Operators

The advection terms are discretized using first-order accurate upwinding,

$$[\mathbf{M}(\mathbf{v})\mathbf{v}]_i^{(1)} = -\left[U_i^+\left(\frac{\widetilde{\nu}_i-\widetilde{\nu}_{i-1}}{\Delta x_i}\right)+U_i^-\left(\frac{\widetilde{\nu}_{i+1}-\widetilde{\nu}_i}{\Delta x_i}\right)\right], \qquad (23)$$

where the advection velocities U^+ and U^- are defined,

$$U_i^+=\frac{1}{2}(U_i+|U_i|), \qquad U_i^-=\frac{1}{2}(U_i-|U_i|). \qquad (24)$$

The Jacobian of the advection operator is,

$$\begin{aligned}\overline{\mathbf{M}}_{i,i-1}^{(1)} &= -(-U_i^+)/\Delta x_i,\\ \overline{\mathbf{M}}_{i,i}^{(1)} &= -(+U_i^+-U_i^-)/\Delta x_i,\\ \overline{\mathbf{M}}_{i,i+1}^{(1)} &= -(+U_i^-)/\Delta x_i.\end{aligned} \qquad (25)$$

Note that $-\overline{\mathbf{M}}^{(1)}$ is M-type and $(\mathbf{M}-\overline{\mathbf{M}})^{(1)}\mathbf{v}=\mathbf{0}$, satisfying the positivity constraints.

Diffusion Operators

We have found that positive operators are more easily constructed if the diffusion terms are rearranged into the form,

$$M(\widetilde{\nu})\widetilde{\nu}=\frac{1+c_{b2}}{\sigma}\nabla\cdot[(\nu+\widetilde{\nu})\nabla\widetilde{\nu}]-\frac{c_{b2}}{\sigma}(\nu+\widetilde{\nu})\nabla^2\widetilde{\nu}, \qquad (26)$$

where liberties have been taken with differentiation of the molecular viscosity ν. The form of (26) avoids discretization of the term $(\nabla\widetilde{\nu})^2$, which does not easily lend itself to positive discrete operators. The diffusion terms are discretized using second-order-accurate central differencing.

$$[\mathbf{M}(\mathbf{v})\mathbf{v}]_i^{(2)} = \frac{1+c_{b2}}{\sigma}\frac{1}{\Delta x_i}\left[(\nu+\widetilde{\nu})_{i+1/2}\frac{\widetilde{\nu}_{i+1}-\widetilde{\nu}_i}{\Delta x_{i+1/2}} - (\nu+\widetilde{\nu})_{i-1/2}\frac{\widetilde{\nu}_i-\widetilde{\nu}_{i-1}}{\Delta x_{i-1/2}}\right], \qquad (27)$$

$$[\mathbf{M}(\mathbf{v})\mathbf{v}]_i^{(3)} = -\frac{c_{b2}}{\sigma}(\nu+\widetilde{\nu})_i\frac{1}{\Delta x_i}* \left[\frac{\widetilde{\nu}_{i+1}-\widetilde{\nu}_i}{\Delta x_{i+1/2}}-\frac{\widetilde{\nu}_i-\widetilde{\nu}_{i-1}}{\Delta x_{i-1/2}}\right]. \qquad (28)$$

The diffusion coefficients $(\nu+\widetilde{\nu})_{i+1/2}$ and $(\nu+\widetilde{\nu})_{i-1/2}$ at cell faces are taken as averages of adjacent cell-centered values,

$$(\nu+\widetilde{\nu})_{i\pm1/2}=\frac{1}{2}[(\nu+\widetilde{\nu})_i+(\nu+\widetilde{\nu})_{i\pm1}], \qquad (29)$$

and $\Delta x_{i+1/2}$ and $\Delta x_{i-1/2}$ are distances between cell centers.

The approximate Jacobians $\overline{\mathbf{M}}^{(2)}$ and $\overline{\mathbf{M}}^{(3)}$ are obtained by freezing the diffusion coefficients,

$$\begin{aligned}\overline{\mathbf{M}}_{i,i-1}^{(2)} &= +\frac{1+c_{b2}}{\sigma}(\nu+\widetilde{\nu})_{i-1/2}\frac{1}{\Delta x_i\Delta x_{i-1/2}},\\ \overline{\mathbf{M}}_{i,i}^{(2)} &= -\frac{1+c_{b2}}{\sigma}(\nu+\widetilde{\nu})_{i-1/2}\frac{1}{\Delta x_i\Delta x_{i-1/2}}\\ &\quad -\frac{1+c_{b2}}{\sigma}(\nu+\widetilde{\nu})_{i+1/2}\frac{1}{\Delta x_i\Delta x_{i+1/2}},\\ \overline{\mathbf{M}}_{i,i+1}^{(2)} &= +\frac{1+c_{b2}}{\sigma}(\nu+\widetilde{\nu})_{i+1/2}\frac{1}{\Delta x_i\Delta x_{i+1/2}}.\end{aligned} \qquad (30)$$

$$\begin{aligned}\overline{\mathbf{M}}_{i,i-1}^{(3)} &= -\frac{c_{b2}}{\sigma}(\nu+\widetilde{\nu})_i\frac{1}{\Delta x_i\Delta x_{i-1/2}},\\ \overline{\mathbf{M}}_{i,i}^{(3)} &= +\frac{c_{b2}}{\sigma}(\nu+\widetilde{\nu})_i\frac{1}{\Delta x_i\Delta x_{i-1/2}}\\ &\quad +\frac{c_{b2}}{\sigma}(\nu+\widetilde{\nu})_i\frac{1}{\Delta x_i\Delta x_{i+1/2}},\\ \overline{\mathbf{M}}_{i,i+1}^{(3)} &= -\frac{c_{b2}}{\sigma}(\nu+\widetilde{\nu})_i\frac{1}{\Delta x_i\Delta x_{i+1/2}},\end{aligned} \qquad (31)$$

These operators satisfy constraint (22a), since

$$[\mathbf{M}-\overline{\mathbf{M}}]^{(2)}\mathbf{v}=\mathbf{0}, \qquad [\mathbf{M}-\overline{\mathbf{M}}]^{(3)}\mathbf{v}=\mathbf{0}. \qquad (32)$$

When negated, the sum $\overline{\mathbf{M}}^{(2)}+\overline{\mathbf{M}}^{(3)}$ forms an M-type matrix. This can be shown by considering individual matrix elements. For example, the sum of the matrix elements above the diagonal becomes.

$$\overline{\mathbf{M}}_{i,i+1}^{(2)}+\overline{\mathbf{M}}_{i,i+1}^{(3)}=\frac{1}{\sigma\Delta x_i\Delta x_{i+1/2}}* \left[(1+c_{b2})(\nu+\widetilde{\nu})_{i+1/2}-c_{b2}(\nu+\widetilde{\nu})_i\right]. \qquad (33)$$

Upon substitution of (29) for the diffusion coefficient at the right cell face, then the sum becomes,

$$\overline{\mathbf{M}}^{(2)}_{i,i+1} + \overline{\mathbf{M}}^{(3)}_{i,i+1} = \frac{1}{2\sigma\Delta x_i \Delta x_{i+1/2}} * \left[(1+c_{b2})(\nu+\tilde{\nu})_{i+1} + (1-c_{b2})(\nu+\tilde{\nu})_i\right]. \quad (34)$$

For $-1 \le c_{b2} \le 1$, these elements are always positive. Similarly, the elements below the diagonal are always positive, and those on the diagonal are always negative. Also, the magnitude of the diagonal elements are equal to the sum of the off-diagonal elements. Hence, the sum $\overline{\mathbf{M}}^{(2)} + \overline{\mathbf{M}}^{(3)}$ is a negated M-type matrix, satisfying constraint (21a).

Baldwin & Barth noted that the steady-state discretization of the diffusion terms in their model must be modified on coarse grids to obtain a non-negative turbulence solution. When written in the form of (26), the diffusion terms of the Baldwin-Barth model give an effective value of c_{b2} below -1. Because of this, they must limit the averaging of the diffusion coefficients to cell faces to ensure their equivalent of $\overline{\mathbf{M}}^{(2)} + \overline{\mathbf{M}}^{(3)}$ is a negated M-type matrix. This limiting procedure reduces spatial accuracy. As shown by the above construction, discretization of the present model's diffusion terms does not require similar modification. The constraint $c_{b2} > -1$, derived on physical grounds, also plays a crucial role in the numerical context.

Source Operators

The production, wall destruction, and transition trip source terms all produce diagonal matrix operators, so grid indices are ignored in the following analysis. Though vector notation is used, all equalities and inequalities apply on a cell-by-cell basis.

The starting point for construction of the implicit source terms $\overline{\mathbf{P}}$ and $\overline{\mathbf{D}}$ is the true Jacobians for the production and destruction operators,

$$[\mathbf{P}(\mathbf{v})\mathbf{v}]' = \mathbf{P}(\mathbf{v}) + \mathbf{P}'(\mathbf{v})\mathbf{v}, \quad (35a)$$
$$[\mathbf{D}(\mathbf{v})\mathbf{v}]' = \mathbf{D}(\mathbf{v}) + \mathbf{D}'(\mathbf{v})\mathbf{v}, \quad (35b)$$

where we use $(\,)'$ for convenience to denote differentiation with respect to $\mathbf{v}$. Also for convenience we define the following operator:

$$\mathrm{pos}(x) = \begin{cases} x & \text{if } x \ge 0 \\ 0 & \text{if } x < 0. \end{cases} \quad (36)$$

Our objective is to choose $\overline{\mathbf{P}}$ and $\overline{\mathbf{D}}$ close to the true Jacobians, namely $[\mathbf{P}(\mathbf{v})\mathbf{v}]'$ and $[\mathbf{D}(\mathbf{v})\mathbf{v}]'$, so that rapid convergence is obtained when the residuals are small, while retaining strict adherence to the positivity constraints for all possible solution states. We give three possible strategies and explain why they are deficient before discussing the strategy we actually employ.

The obvious choice of setting the implicit operators equal to their true Jacobians does not satisfy the positivity constraints. For example, $[\mathbf{P} - \overline{\mathbf{P}}]\mathbf{v} \ge 0$ is not met if $\mathbf{P}' > \mathbf{0}$.

A second strategy, which always satisfies the M-type matrix constraints, is to take the negative part of the production Jacobian and the positive part of the destruction Jacobian,

$$\overline{\mathbf{P}} = -\mathrm{pos}[-\mathbf{P} - \mathbf{P}'\mathbf{v}], \quad (37a)$$
$$\overline{\mathbf{D}} = \mathrm{pos}[\mathbf{D} + \mathbf{D}'\mathbf{v}]. \quad (37b)$$

This strategy is also defective and must be discarded because the other two positivity constraints may not be met. For example, if $\mathbf{D} > \mathbf{0}$ and $\mathbf{D}' < \mathbf{0}$, then $\mathbf{D} - \overline{\mathbf{D}} \le \mathbf{0}$ will not be satisfied.

A third strategy is to use only the negative parts of $\mathbf{P}$ and $\mathbf{P}'$ in (35a) to form $\overline{\mathbf{P}}$, and the positive parts of $\mathbf{D}$ and $\mathbf{D}'$ in (35b) to form $\overline{\mathbf{D}}$,

$$\overline{\mathbf{P}} = -\mathrm{pos}[-\mathbf{P}] - \mathrm{pos}[-\mathbf{P}']\mathbf{v}, \quad (38a)$$
$$\overline{\mathbf{D}} = \mathrm{pos}[\mathbf{D}] + \mathrm{pos}[\mathbf{D}']\mathbf{v}. \quad (38b)$$

This is a viable strategy; the four source term positivity constraints are satisfied for all possible sign combinations of $\mathbf{P}$, $\mathbf{P}'$, $\mathbf{D}$ and $\mathbf{D}'$. However, we discard this strategy because of its slow convergence rate.

In a typical flow situation, both production and destruction increase in magnitude as $\tilde{\nu}$ is increased (i.e., $\mathbf{P}$, $\mathbf{D}$ and their derivatives are all positive). In this case our third strategy chooses,

$$\overline{\mathbf{P}} = 0, \qquad \overline{\mathbf{D}} = \mathbf{D} + \mathbf{D}'\mathbf{v} = [\mathbf{D}(\mathbf{v})\mathbf{v}]'. \quad (39)$$

This is equivalent to integrating the production term explicitly and the destruction term implicitly; this technique has often been used for solution of k-ϵ models. Although this strategy guarantees positivity, it can result in extremely slow convergence in regions where production and destruction are large and dominate the equation budget. In these regions, the Jacobians $[\mathbf{P}(\mathbf{v})\mathbf{v}]'$ and $[\mathbf{D}(\mathbf{v})\mathbf{v}]'$ will be individually large but will tend to cancel. Now if only $[\mathbf{D}(\mathbf{v})\mathbf{v}]'$ is used to update the solution, then the contribution to the diagonal element of the matrix will be excessive; the resulting solution change $\Delta\mathbf{v}$ will be correspondingly small even when the residuals are not close to zero.

This possible analytic cancellation of the individually large Jacobians motivates our final strategy for choosing the implicit source terms. Rather than concentrating on the individual production and destruction Jacobians, we consider the source terms combined together and use a variation of (38),

$$\overline{\mathbf{D}} - \overline{\mathbf{P}} = \mathrm{pos}[\mathbf{D} - \mathbf{P}] + \mathrm{pos}[\mathbf{D}' - \mathbf{P}']\mathbf{v}. \quad (40)$$

With the source terms taken together, only two positivity constraints are required,

$$\overline{\mathbf{D}} - \overline{\mathbf{P}} \geq \mathbf{0}, \tag{41a}$$

$$[\overline{\mathbf{D}} - \mathbf{D}] - [\overline{\mathbf{P}} - \mathbf{P}] = [\overline{\mathbf{D}} - \overline{\mathbf{P}}] - [\mathbf{D} - \mathbf{P}] \geq \mathbf{0}. \tag{41b}$$

Examining the four possible sign combinations for $[\mathbf{D} - \mathbf{P}]$ and $[\overline{\mathbf{D}} - \overline{\mathbf{P}}]$, these positivity constraints are always satisfied by (40). Furthermore, analytic cancellation of production and destruction is reflected in (40), resulting in superior convergence compared to (38).

We evaluate the Jacobians $\mathbf{P}'$ and $\mathbf{D}'$ analytically using the chain rule. The differentiation is straightforward, except for the wall destruction term f_w. Since evaluation and differentiation of f_w involves terms like r^{-6} and r^{12}, care must be taken for r small or large, lest one's computer begins to complain. The form of (6) gives acceptable numerical behavior for $r \to 0$. For large r, the function f_w asymptotes to $[1 + c_{w3}^6]^{1/6}$, so above some cutoff (say $r = 10$), the derivative $(f_w)'$ is set to zero.

Approximate Factorization

With the implicit and explicit operators properly defined, the backward Euler solution procedure (18) guarantees a positive turbulence field at each update. It does, however, require expensive inversion of a large sparse matrix in 2-D or 3-D. Approximate factorization of the implicit operator will reduce the cost of an update, but unconditional positivity is lost. To see this effect consider a 2-D flow with zero source terms. The unsplit implicit system is,

$$\left[\mathbf{I} - \Delta t \left(\overline{\mathbf{M}}_\xi + \overline{\mathbf{M}}_\eta\right)\right] \Delta \mathbf{v}^n = \Delta t \left(\mathbf{M}_\xi + \mathbf{M}_\eta\right) \mathbf{v}^n, \tag{42}$$

where $\mathbf{M}_\xi$ and $\mathbf{M}_\eta$ are finite differences in the ξ and η coordinate directions, respectively, and $\overline{\mathbf{M}}_\xi$ and $\overline{\mathbf{M}}_\eta$ satisfy the positivity constraints (21a) and (22a). If the implicit operator is approximately factorized, then the system becomes,

$$\left[\mathbf{I} - \Delta t \overline{\mathbf{M}}_\xi\right] \left[\mathbf{I} - \Delta t \overline{\mathbf{M}}_\eta\right] \Delta \mathbf{v}^n = \Delta t \left(\mathbf{M}_\xi + \mathbf{M}_\eta\right) \mathbf{v}^n. \tag{43}$$

Rearranging this system to isolate $\mathbf{v}^{n+1}$ gives,

$$\left[\mathbf{I} - \Delta t \overline{\mathbf{M}}_\xi\right] \left[\mathbf{I} - \Delta t \overline{\mathbf{M}}_\eta\right] \mathbf{v}^{n+1} = \left[\mathbf{I} + \Delta t (\mathbf{M}_\xi - \overline{\mathbf{M}}_\xi) + \Delta t (\mathbf{M}_\eta - \overline{\mathbf{M}}_\eta) + \Delta t^2 \overline{\mathbf{M}}_\xi \overline{\mathbf{M}}_\eta\right] \mathbf{v}^n. \tag{44}$$

The splitting error results in the term $\Delta t^2 \overline{\mathbf{M}}_\xi \overline{\mathbf{M}}_\eta \mathbf{v}$, which may not be positive. For small enough Δt the splitting error will not ruin positivity, but the constraint equation on Δt is a nonlinear matrix equation in itself and is quite difficult to solve.

We conclude that there appears to be no approximate factorization of (18) that retains the unconditional positivity of the original unsplit system. We propose using subiterations of an approximate factorization scheme at each time step, which will recover the update of the original unsplit system at convergence (of the subiteration process). We use the subiteration process of Steinthorsson & Shih [22], where the splitting error is simply lagged one subiteration. The objective of the approximate factorization is then to minimize splitting error for rapid convergence, and to minimize the number of subiterations where the candidate updated field contains negative points.

In 2-D we have tried conventional ADI with an additional factor due to the source terms,

$$\left[\mathbf{I} - \Delta t \overline{\mathbf{M}}_\xi\right] \left[\mathbf{I} - \Delta t \overline{\mathbf{M}}_\eta\right] \left[\mathbf{I} - \Delta t (\overline{\mathbf{P}} - \overline{\mathbf{D}})\right] \Delta \mathbf{v}^n = \Delta t \mathbf{R} \mathbf{v}^n, \tag{45}$$

where $\mathbf{R}$ is the residual or right-hand-side operator in (18). We have also tried the approximate factorization developed by Shih & Chyu [23] for finite-rate chemistry,

$$\left[\mathbf{N} - \Delta t \overline{\mathbf{M}}_\xi\right] \mathbf{N}^{-1} \left[\mathbf{N} - \Delta t \overline{\mathbf{M}}_\eta\right] = \Delta t \mathbf{R} \mathbf{v}^n, \tag{46a}$$

$$\mathbf{N} \equiv \mathbf{I} - \Delta t (\overline{\mathbf{P}} - \overline{\mathbf{D}}). \tag{46b}$$

As discussed in [23], this second form has lower splitting error and converges much faster to the unsplit update than conventional ADI. However, even this second form requires several subiterations at start up to achieve a non-negative updated turbulence field; for example, approximately 30 subiterations are needed for a time step of $\Delta t = 10$ (based on chord and freestream density and pressure) to eliminate all negative updated points.

We use an approximate factorization that outperforms both (45) and (46). Prior to splitting, we divide through by the diagonal element of the implicit operator, then use a conventional approximate factorization. Denoting the diagonal elements of the implicit advection/diffusion operators as $\overline{\mathbf{M}}_\xi^{(d)}$ and $\overline{\mathbf{M}}_\eta^{(d)}$, the scheme becomes,

$$\left[\mathbf{I} - \Delta t \tilde{\overline{\mathbf{M}}}_\xi\right] \left[\mathbf{I} - \Delta t \tilde{\overline{\mathbf{M}}}_\eta\right] \Delta \mathbf{v}^n = \Delta t \tilde{\mathbf{R}} \mathbf{v}^n, \tag{47}$$

where

$$\begin{aligned} \tilde{\overline{\mathbf{M}}}_\xi &= \left[\mathbf{I} - \Delta t (\overline{\mathbf{M}}_\xi^{(d)} + \overline{\mathbf{M}}_\eta^{(d)} + \overline{\mathbf{P}} - \overline{\mathbf{D}})\right]^{-1} \left[\overline{\mathbf{M}}_\xi - \overline{\mathbf{M}}_\xi^{(d)}\right], \\ \tilde{\overline{\mathbf{M}}}_\eta &= \left[\mathbf{I} - \Delta t (\overline{\mathbf{M}}_\xi^{(d)} + \overline{\mathbf{M}}_\eta^{(d)} + \overline{\mathbf{P}} - \overline{\mathbf{D}})\right]^{-1} \left[\overline{\mathbf{M}}_\eta - \overline{\mathbf{M}}_\eta^{(d)}\right], \\ \tilde{\mathbf{R}} &= \left[\mathbf{I} - \Delta t (\overline{\mathbf{M}}_\xi^{(d)} + \overline{\mathbf{M}}_\eta^{(d)} + \overline{\mathbf{P}} - \overline{\mathbf{D}})\right]^{-1} \mathbf{R}. \end{aligned} \tag{48}$$

We incorporate this approximate factorization scheme into a subiteration process in the fashion of Steinthorsson & Shih [22], where the splitting error $\Delta t^2 \tilde{\overline{\mathbf{M}}}_\xi \tilde{\overline{\mathbf{M}}}_\eta \Delta \mathbf{v}$ is lagged one subiteration,

$$\begin{aligned} \left[\mathbf{I} - \Delta t \tilde{\overline{\mathbf{M}}}_\xi\right] \Delta \mathbf{v}^{*(k)} &= \Delta t \tilde{\mathbf{R}} \mathbf{v}^n - \Delta t \tilde{\overline{\mathbf{M}}}_\xi \left(\Delta \mathbf{v}^* - \Delta \mathbf{v}\right)^{(k-1)} \\ \left[\mathbf{I} - \Delta t \tilde{\overline{\mathbf{M}}}_\eta\right] \Delta \mathbf{v}^{(k)} &= \Delta \mathbf{v}^{*(k)} \end{aligned} \tag{49}$$

The second step equation has been used to rewrite the splitting error on the right-hand side in the first step; Δv^* is a convenient definition.

In practice this splitting performs quite well. Using a constant Δt throughout the field, we have yet to encounter a situation where a negative turbulence update occurs even on the first subiteration. This includes tests where Δt was varied over several orders between 0.001 and 1000.

From numerical experimentation, we choose $\Delta t = 10$ and stop subiterating when the normalized change $||\Delta\tilde{\nu}/(\nu + \tilde{\nu})||_2$ is reduced below 0.01. Typically, 10 to 20 subiterations are needed for initialization transients and approximately 30 are required when the transition trip function "wakes up". Within a few time steps only one subiteration is needed.

This procedure of dividing through by the diagonal elements also improves the scheme's resistance to round-off error in the inviscid region where $\tilde{\nu}$ is small. The solution module will still function properly if the freestream $\tilde{\nu}_\infty$ or the initial guess for $\tilde{\nu}$ is set to zero. In comparison, round-off errors may cause negative updates, even at convergence of the subiterations, if either (45) or (46) is used.

The model shows promising convergence to steady-state when coupled to the solver for the velocity field. Convergence is typically as good or better than that for the Baldwin-Lomax algebraic model. This may be due to the absence of "blinking" phenomenon in the present model. In algebraic models, convergence to steady-state may be adversely affected by discontinuous behavior. For example, the position where the eddy viscosity switches between inner and outer formulations may wander back and forth between adjacent cells, slowing convergence or causing a limit cycle.

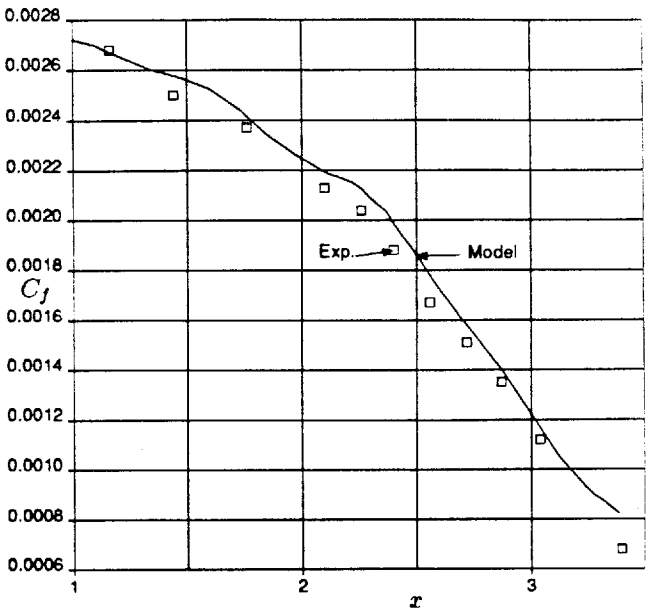

Figure 7: Ski-friction coefficient in Samuel-Joubert flow, based on $U_{\infty 0}$. x in meters.

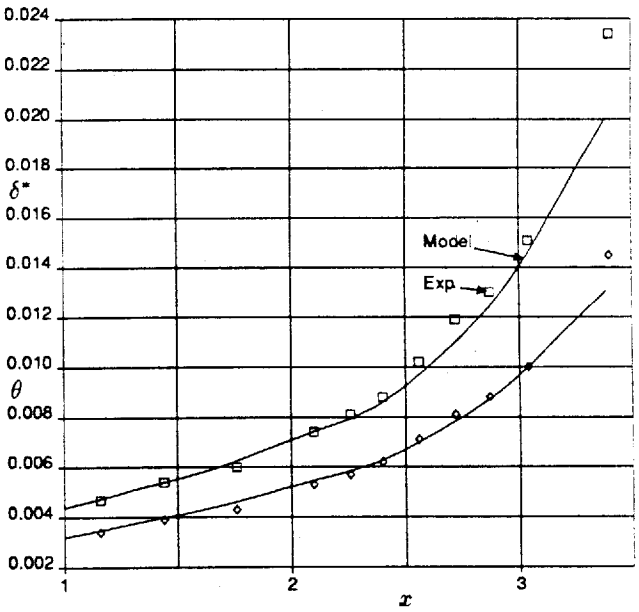

Figure 8: Momentum and displacement thicknesses in Samuel-Joubert flow, in meters.

Results

Boundary-Layer Calculations

Only incompressible boundary layers have been considered. With zero pressure gradient, the model obeys the accepted Reynolds-number scaling, so the results shown at $R_\theta = 10^4$ ensure agreement with the current theories. The model gives satisfactory results in attached boundary layers with pressure gradients, typical of the Stanford 1968 cases. We only present results for the sink flow and the Samuel-Joubert flow [24] as the other cases with moderate gradients show the same trend. Darmofal's code was used again.

In the sink flow, with an acceleration parameter $K \equiv \nu/U_\infty^2(dU_\infty/dx)$ equal to 1.5×10^{-6}, we obtain $C_f = 0.00535$, $H = 1.35$, and $R_\theta = 760$. These results are well within the experimental range, which is about $[0.0050, 0.0057]$ for C_f, $[1.35, 1.42]$ for H, and $[700, 800]$ for R_θ. The eddy-viscosity profile is atypical. Because of the lack of entrainment in the sink flow, it does not show a front at the edge of the boundary layer. Instead, it extends into the freestream region. This did not disturb the velocity profile, which is satisfactory both in terms of thickness and shape.

In the Samuel-Joubert flow the agreement is rather good for the skin friction, Fig. 7, and the thicknesses,

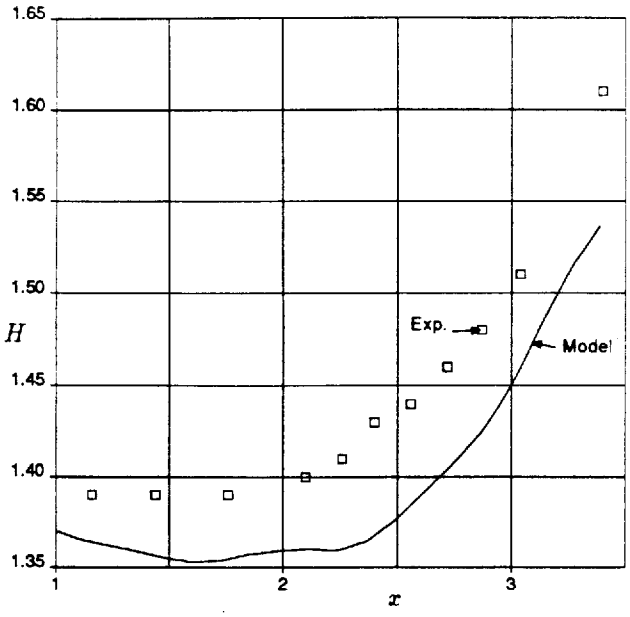

Figure 9: Shape factor in Samuel-Joubert flow.

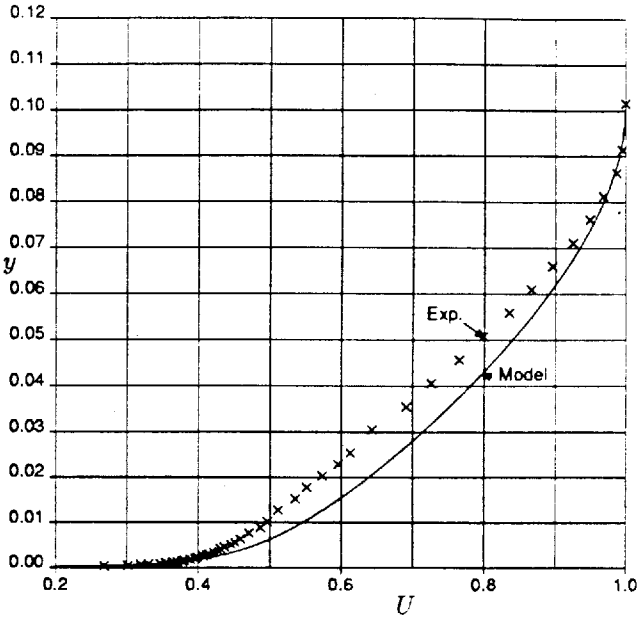

Figure 10: Velocity profile at $x = 3.4$m in Samuel-Joubert flow. U normalized with edge velocity. y in meters.

Fig. 8. The model produces slightly higher skin friction, but lower thicknesses. The shape factors (Fig. 9) are in disagreement even before the pressure gradient is applied, and are the root of the disagreement in thicknesses. With an adverse gradient, the skin-friction term loses its authority in the momentum equation. The experimental values for x between 1 and 2m, $H \approx 1.39$, are surprisingly high considering the weak pressure gradient and the Reynolds number, $R_\theta \approx 6500$. Interestingly, the calculated shape factor is catching up with the experimental one for $x > 3$m.

Figure 10 shows the velocity at $x = 3.4$m. The position of the boundary-layer edge is good, but the computed profile is fuller than the experimental profile. The shear-stress profiles in Fig. 11 show good agreement for the outer values, but the near-wall agreement may be poor enough to partly explain the differences in the velocity profiles. Stress disagreements can of course be compounded by the convection and pressure terms. Curiously Dr. F. Menter, who was kind enough to test the model in his Navier-Stokes code [25], obtained similar agreement for the stress profiles, but better agreement for the velocity.

The Samuel-Joubert results suggest a mild but genuine tendency to underpredict the shape factor and thicknesses in adverse pressure gradients. This may make the model a little more resilient to separation than it would ideally be. The tendency is not as strong as with the Cebeci-Smith, Baldwin-Lomax, and k-ϵ models, but our comparison with experiment is not quite as good as that obtained by Menter with the Johnson-King and k-ω models [25]. Both models have been finely tuned over years, with an emphasis on precisely

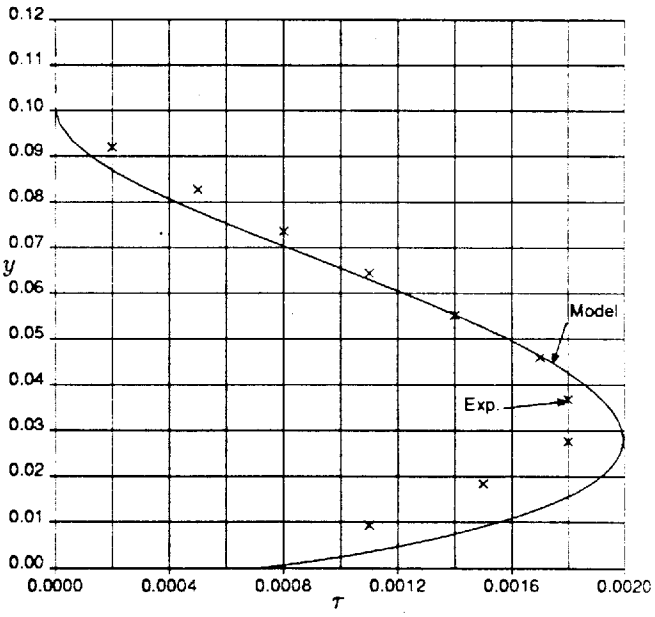

Figure 11: Shear-stress profile at $x = 3.39$m in Samuel-Joubert flow. τ normalized with edge velocity. y in meters.

this type of flow. Nevertheless, the behavior of the new model is not disappointing and vindicates the notion that a model calibrated for mixing layers, wakes, and zero-gradient boundary layers has a good chance in adverse-gradient boundary layers, which are an intermediate situation. In addition, an improvement of the destruction term may yet be found sufficient to obtain results on a par with the best models.

Navier-Stokes Calculations

We present three cases of the RAE 2822 airfoil; the first two have a sharp trailing edge but shock interactions of different strengths, and the third has a blunt trailing edge.

Navier-Stokes calculations for Cases 6 and 10 on the RAE 2822 airfoil [26] were performed using the present model, as well as the Baldwin-Lomax and Johnson-King turbulence models. The Johnson-King results were obtained using the Navier-Stokes code of Swanson [27]. Results for each model were computed on 384×80 and 768×160 grids to minimize numerical errors. These grids were generated by the elliptic method of Wigton [28]. The medium and fine grids contain 257 and 513 points on the airfoil, respectively.

All calculations for Case 6 were performed at the same conditions: $M = 0.725$, $Re = 6.5 \times 10^6$, a prescribed lift coefficient of $Cl = 0.743$, and transition trips at 3% chord. Results on the 768×160 grid are shown in Figs. 12 and 13. All models converged solidly on both grids.

Figure 12 shows a comparison of surface pressures for Case 6 obtained with the three turbulence models and experiment [26]. The shock for the present model is about 1.5% chord farther forward than in the experiment or as predicted with the Baldwin-Lomax and Johnson-King models, but well within the scatter of various models as reported at the Viscous Transonic Airfoil Workshop (VTAW) [6]. The new model is farther from the experiment near the leading edge on the upper surface, but closer to the experiment near the trailing edge on the lower surface. All the calculations reveal small pressure glitches near the trailing edge. With the new model on the fine grid, the angle of attack was 2.37°, the drag coefficient 0.0121, and the moment coefficient -0.091, compared with 2.92°, 0.0127, and -0.095 in the experiment, respectively.

Figure 13 shows the upper-surface skin-friction coefficient for the same case. Between the three models there is a difference of up to 10% upstream of the shock, and similar but reversed differences downstream of it. The new model does not predict wall-shear reversal. The other two predict reversal at the foot of the shock, but only on the finest grid (768×160). Reversal was never predicted at the VTAW, where the finest grid used was 369×65. It appears that with current codes the simple question of whether reversal occurs is not firmly answered even at grid resolutions that are considered very fine. At the shock, the new model produces a larger step up for the boundary-layer thicknesses than with Baldwin-Lomax, resulting in a more forward position. Interestingly, the size of the displacement effect is not correlated with the occurrence of reversal at the wall.

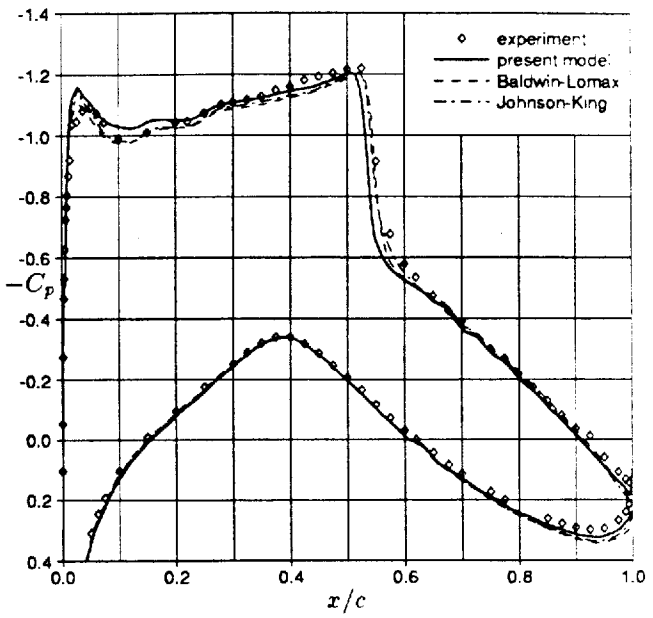

Figure 12: Pressure distribution for Case 6, RAE 2822 airfoil.

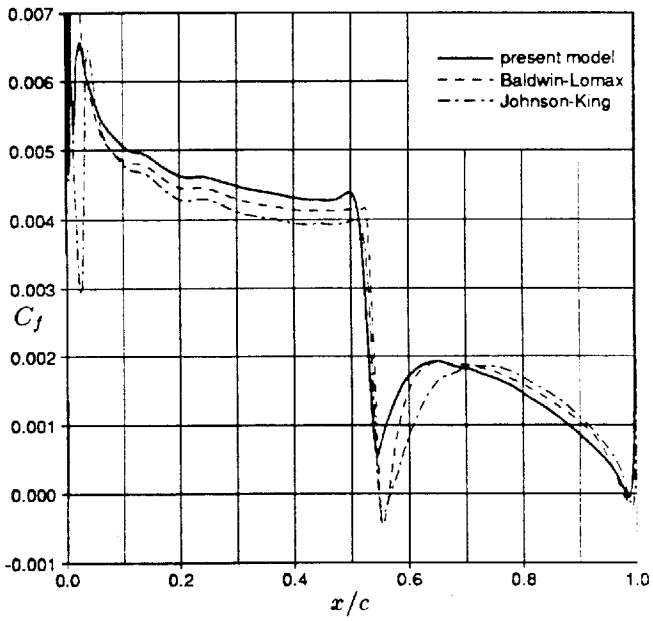

Figure 13: Skin-friction coefficient on upper surface for Case 6, RAE 2822 airfoil. C_f based on U_∞.

Flow conditions for the RAE 2822 Case 10 are $M = 0.75$, $Re = 6.5 \times 10^6$, a prescribed lift coefficient of $Cl = 0.743$, and trips at 3% chord. The new model obtained a steady solution on the 384×80 grid, but produced a limit cycle on the finer 768×160 grid. All the cyclic variation was in the separation bubble. The new model also produced a limit cycle on the 384×80 grid when the artificial dissipation in the Navier-Stokes solver was cut in half. Baldwin-Lomax and Johnson-

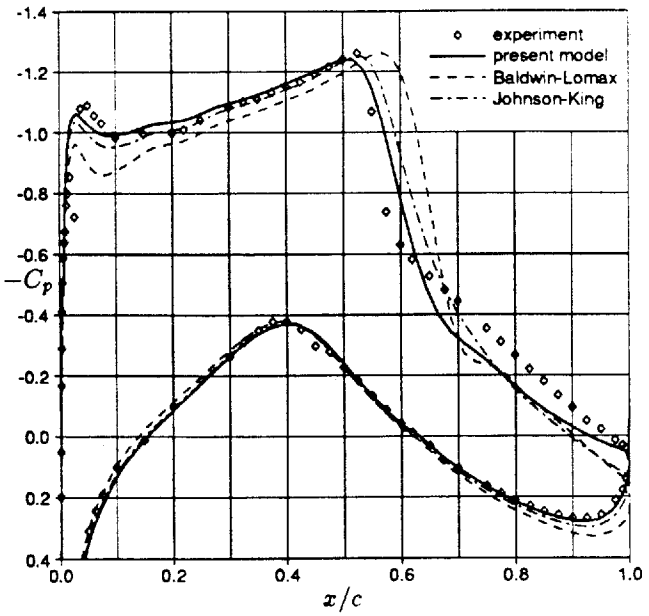

Figure 14: Pressure distribution for Case 10, RAE 2822 airfoil.

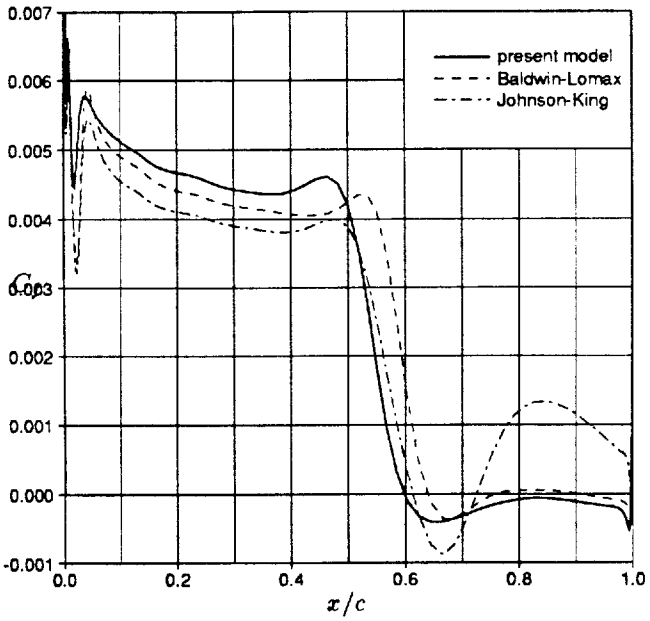

Figure 15: Skin-friction coefficient on upper surface for Case 10, RAE 2822 airfoil. C_f based on U_∞.

King produced steady solutions on both grids. Results for Case 10 are presented in Figs. 14 and 15 for all three turbulence models on the 384 × 80 grid.

As usual, Case 10 produces larger differences than Case 6. With our policy of matching the Mach number and lift coefficient the new model gives a better answer than Baldwin-Lomax, and slightly better than Johnson-King (see Fig 14). This is in terms of shock location and pressures near the leading edge, upper surface, and trailing edge, lower surface. All the models fail to agree with experiment for $x/c > 0.7$, upper surface. The new model predicts a flattening pressure for $x/c > 0.9$, upper surface, in qualitative disagreement with the experiment. The Johnson-King model has shown the same trend, but not as strongly and only in Coakley's implementation [6]. The Baldwin-Barth model also produces the flattening [8].

This behavior of the C_p is correlated with that of the skin-friction coefficient, Fig. 15. Downstream of the shock, the experiment and our Johnson-King results show the skin friction returning to strong positive values. The flow reattaches firmly. The Baldwin-Lomax results show weakly positive skin friction over a short stretch. With the new model the skin friction grazes zero before again taking moderate negative values. There is no reattachment, and the flattening pressure distribution reflects it. Note that a similar behavior has been observed with algebraic models: if the skin friction approaches zero smoothly enough the Van-Driest damping can, erroneously, "shut down" the eddy viscosity across the whole layer. This is not what is happening here.

The limit cycle behavior of the new model on the fine grid shows an oscillation between slightly negative and slightly positive skin friction near $x/c = 0.8$.

The apparent failure to reattach is not a favorable result, and this behavior was also observed in another separated case (B. Paul, personal communication). The solutions show a very low eddy viscosity near the wall. A run with a more diffusive model (i.e., lower σ) that could have helped the eddy viscosity diffuse towards the wall failed to show much difference. However we do not believe there is a structural reason for the failure to reattach, based on two tests. The first is a calculation of reattachment on our boundary-layer code, modified to a time-developing code; a layer of reversed flow near the wall was eliminated as could be expected. The second is an unpublished calculation by Menter of a separation bubble; again the skin friction returned to positive values without hesitation. Numerical errors in our current Navier-Stokes/turbulence-model solver may be playing a role.

For Case 10, with the new model on the 384 × 80 grid, the angle of attack was 2.52°, the drag coefficient 0.0238, and the moment coefficient −0.104, compared with 3.19°; 0.0242, and −0.106 in the experiment, respectively.

The blunt-trailing edge airfoil is RAE 2822, truncated at 94% of the original chord (base height 1.14% chord). Our objective is to explore the behavior of the model and of the numerics at corner-induced separation, with high-lift applications in mind. Accordingly we chose Case 1 [29] which is subcritical: $M = 0.676$, $Re = 5.4 \times 10^6$, and lift coefficient $Cl = 0.451$. Calculations

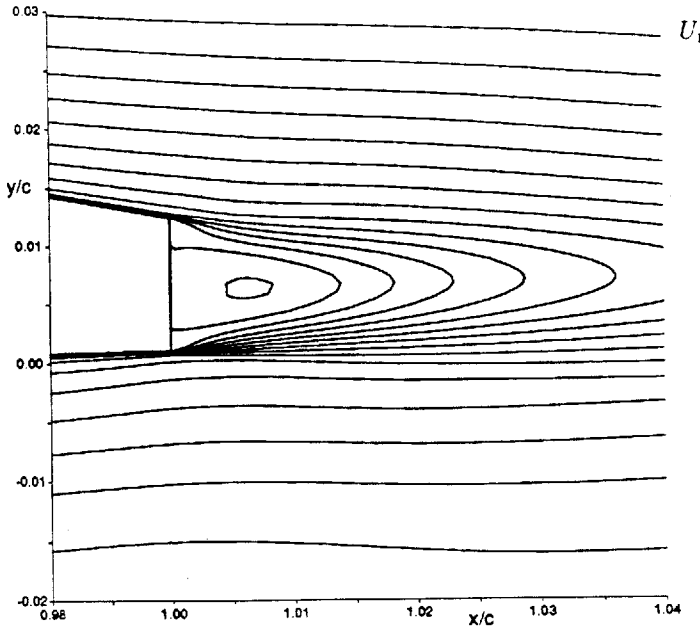

Figure 16: Velocity contours near the trailing edge for Case 1, blunt RAE 2822 airfoil. Levels: −0.007 (small island), 0., 0.007...

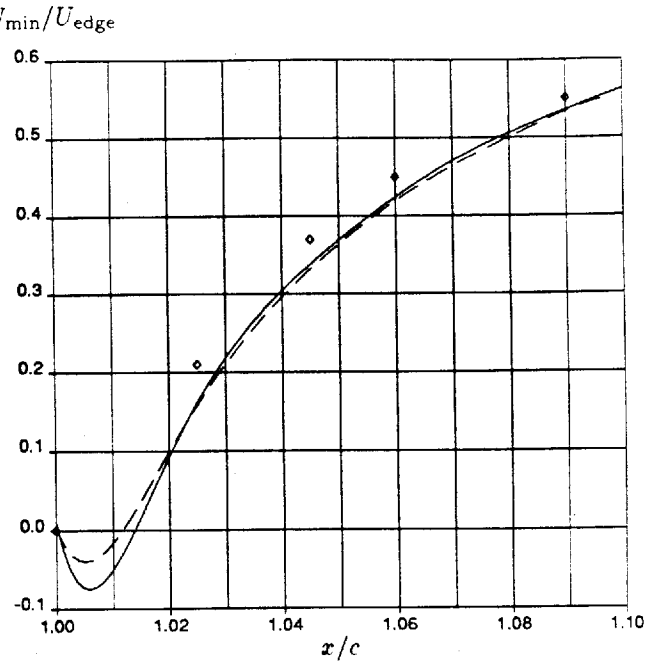

Figure 17: Minimum velocity in wake for Case 1, blunt RAE 2822 airfoil. ◇ experiment, − − − 768 × 160 grid, − − − 384 × 80 grid.

were performed on medium and fine two-block grids. The fine grid consists of a 768 × 160 C-grid block around the airfoil and a 128 × 64 block downstream of the blunt trailing edge. The grid contains 513 points on the airfoil and 65 points across the blunt base. The medium grid contains blocks of 384 × 80 and 64 × 32. Results for Case 1 are presented for the fine grid.

Strong convergence was obtained, and solution glitches are less severe than with the sharp trailing edge. The angle of attack for Case 1 is 2.035°, the drag coefficient 0.0097, and the moment coefficient −0.061, compared with 2.45°, 0.0098, and −0.060 in the experiment, respectively.

In another example of slow convergence of the detail features in the flow, the amplitude of the backflow doubles between the 384 × 80 grid and the 768 × 160 grid. The region with negative velocities extends a little over one step height (i.e., 1.35% on the fine grid, the step being 1.14% chord) beyond the trailing edge. The report on the experiment also shows about 1.2 step heights, but the interpolation is debatable in that the $U = 0$ line is shown with an apex, probably due to the understandable sparsity of the measurements. The region of reversed flow should not be confused with the displacement body invoked in integral boundary-layer methods, which tends to be much longer (2.5 to 5 step heights). Figure 16 shows velocity contours, with the expected wedge-shaped region of low velocity. Figure 17 shows the minimum velocity in the wake, which is in fair agreement with the experiment [29]. The computed curve is shifted by about 0.5% chord downstream. This suggests

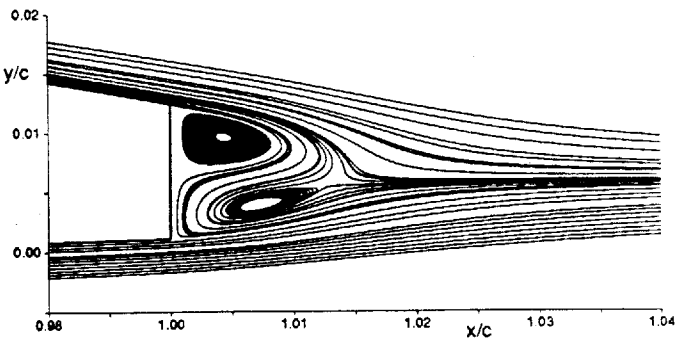

Figure 18: Streamlines near the trailing edge for Case 1, blunt RAE 2822 airfoil.

that the model not only gives an accurate growth rate for a fully-developed wake (per its calibration), but is also fairly accurate for a "young", asymmetric one. The wake of a wing, which is combined with a mixing layer, is still a different problem; nevertheless, we expect the model should also be able to treat it well.

Figure 18 shows streamlines (but not equally-spaced stream-function contours). Their pattern is unexpected, being rather asymmetric and indicating "reattachment" of an upper-surface streamline near the mid-point of the base. There are three half-saddles, one saddle, and two nodes. This differs from the "educated guess" made, for instance, in [30]. That guess assumes that the streamlines connected to the three half-saddles meet at the full

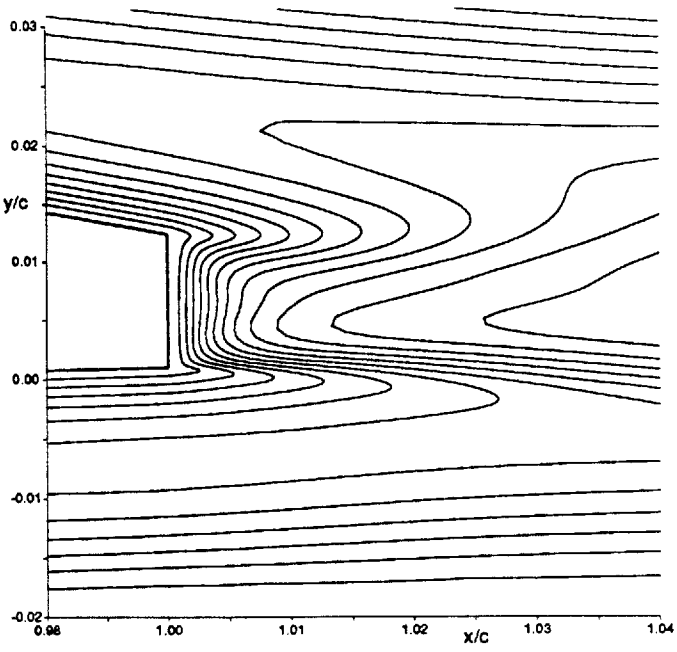

Figure 19: Eddy-viscosity contours near the trailing edge for Case 1, blunt RAE 2822 airfoil.

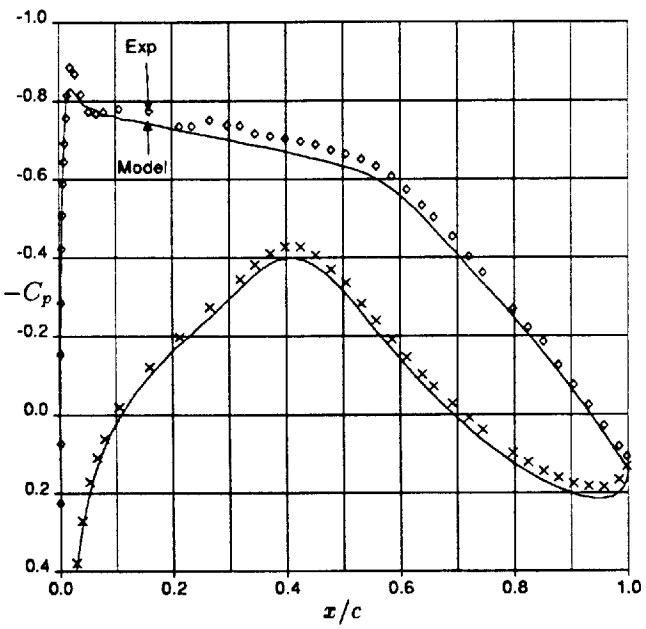

Figure 20: Pressure distribution for Case 1, blunt RAE 2822 airfoil.

saddle, isolating the two nodes. There is no reason for such a pattern to occur in the absence of symmetry, and it is not stable. The saddle and the lower node could also eliminate each other under other conditions. Streamline patterns can overstate the importance of regions with low velocity and little dynamical significance.

Figure 19 shows eddy-viscosity contours. Continuity between the grid blocks, which is hard to achieve with algebraic models, is of course observed. The eddy viscosity blends its boundary-layer behavior (as in Fig. 4) into its wake behavior (a bell-shaped distribution). There is little basis to judge its level in the recirculation region.

Finally Fig. 20 shows the pressure distribution. The agreement is good, especially considering the 0.415° difference in angle of attack, except that the calculated C_p is shifted down. This was also observed by Drela for his numerical method [31]. We also ran Case 4 to measure the Reynolds-number effect. In the experiment, Case 4 had the same angle of attack as Case 1, but a Reynolds number of only 1.9×10^6, resulting in a loss of 0.036 in C_l. We ran Case 4 with imposed $C_l = 0.415$, and the angle of attack settled at 1.94°. The lift-curve slope is about 0.155 per degree. This implies that the C_l loss due to the lower Reynolds number is about 0.022. This is only about 60% of the lift loss observed in the experiment.

Summary of the results

We have exercised the model outside its domain of calibration and with the full Navier-Stokes equations, instead of just the boundary-layer equations. Its compatibility with unstructured grids has yet to be used, but there is no need to demonstrate it. In a few cases with shock-induced separation the new model yielded a limit cycle, with a pulsation of the bubble, when the algebraic models yielded steady solutions. Since time-accurate solutions are very expensive, steady solutions may be greeted as successes whether they are physically correct or not. Outright divergence of the iterative process has never occurred, and the model seems to be reasonably "friendly" to the relaxation process, without any attention being paid to the initial condition. Thus, the model appears robust enough to be implemented by independent users, in a variety of codes and physical situations, and it should be particularly attractive to unstructured-grid users.

The accuracy so far is consistent with our expectations. The model's response to gradual or steep pressure gradients, and to the removal of the blocking effect of the wall, is encouraging. The post-shock reattachment in an adverse pressure gradient has proven to be difficult for the model. Menter also reported somewhat disappointing results over a backward-facing step, traced to an excessively-rapid build-up of the shear stress (personal communication). This weakness also afflicts the k-ϵ model, and may respond to a modification of the f_w function. The quality of our results with the blunt trailing edge indicate that this problem cannot be very severe. It appears that the calibration cases are indeed representative enough of the flows of interest to ensure decent performance in non-trivial situations, and to warrant extensive applications and tests of the model in its present form.

Outlook

The development of the model will nevertheless continue. It will preserve the basic favorable features of the model: single transport equation, local formulation, moderate resolution requirements, good numerical stability, insensitivity to the freestream value, ready control of transition. The invariance principles will also be upheld. Additional tests will be made, notably in three dimensions. No additional difficulties are anticipated. Tests in more strongly stimulated flows such a massive separation, wakes in pressure gradients, or free vortices, are likely to reveal weaknesses in the model. They will also stress the current Navier-Stokes codes, in two respects. The first is the detail accuracy, for instance the conservation of momentum in boundary layers, which is far from perfect in our experience. This problem has been obstructed by the difficulty in computing the thicknesses δ^* and θ in Navier-Stokes codes, but it must now be addressed, if only on a flat plate at low Mach number.

The other aspect is the question of steady solutions in flows with medium- or large-scale separation. An classic example is the flow past a circular cylinder; a pressing industrial example is the flow past a stalled airfoil, near its maximum lift coefficient $C_{l,max}$. Except at very low Reynolds number the flow is unsteady and three-dimensional. On the other hand, provided the geometry is time-independent, it is legitimate to define its time-average and to hope for a code that would compute it as a steady solution. It is *also* legitimate to request the low-frequency component (i.e., with Strouhal number of order 1) of the solution, particularly the fluctuating loads for structural purposes. The ideal turbulence would include a switch between these two options. We do not know, in general, whether the exact solution of the Navier-Stokes/turbulence-model system in its present form is steady. In the design of some models, decisions have been made solely on the basis of a preference for the candidate that yielded steady solutions. We are far from having the capability of routinely performing time-accurate calculations to explore the issue. All the routine calculations aim at steady solutions. Failure to converge, and the generation of a limit cycle, *may* be a sign that the exact solution is unsteady. It may also be just a numerical problem.

Envision a steady solution, say past a cylinder. An algebraic model such as, for instance, Baldwin-Lomax would be used out of its range, but this does not stop eager users. In the recirculating region it would yield eddy viscosities on the order of $U_\infty R$, with U_∞ the freestream velocity and R the cylinder radius. We presume here that the Baldwin-Lomax f_{max} condition would occur in the wake, and not near the wall. A balance between production, on one side, and diffusion and destruction, on the other, suggests that the new model also could produce a solution with an eddy viscosity of order $U_\infty R$ in the recirculation region. A Reynolds number based on that viscosity would be finite, which shows that there is no immediate scaling argument that can predict whether a steady solution can be stable. This question must await extensive tests. The pressure to produce time-accurate Navier-Stokes codes will only increase, even if the steady-state codes have not reached perfection.

Even when unsteady solutions of the modeled equations are obtained, their meaning will need scrutiny. Many of the properties of Reynolds-averaging hold approximately if there is a separation of scales (i.e., a spectral gap) between the resolved motions and those that are left to the turbulence model. We have little evidence in that domain. An example of legitimate decomposition would be a mixing layer that wanders on a time scale much longer that its internal time scale which, after modeling, is $\delta/\Delta U$ (with δ the thickness, and ΔU the velocity difference). Note that what we envision here is different from Large-Eddy Simulation. As the grid is refined the model does not change, the way it does in LES (through a narrowing of the filter, so that the limit is direct simulation). The difficulty of LES is the filtering without spectral gap. Instead, we converge to a smooth solution of the modeled equations.

Some of the near-future directions have been hinted at above. There is the choice of S, between the vorticity, the strain rate, or another scalar norm of the deformation tensor. There is the use of an approximation of the turbulent kinetic energy k to give the Reynolds-stress tensor a plausible trace (or set of eigenvalues). There is a modification of the f_w function in the region $r > 1$, that would alter the results only on adverse pressure gradients. The third modification could be assessed in the Samuel-Joubert or airfoil flows, but obvious test cases for the first two are not at hand.

The current model has no compressibility terms. Empirical terms based on the turbulent Mach number, such as the one in the Secundov model, or on the quantity $\nabla\rho.\nabla\tilde{\nu}$ are available. The former may be calibrated in supersonic mixing layers. The latter may assist the model in shock/boundary-layer interactions if a consistent trend is found that shows an erroneous shock location, and we can extricate that trend from numerical concerns (e.g., artificial dissipation) and from the endless corrections of transonic airfoil testing. In that range of density variations it may be enough to write the transport equation in terms of $\tilde{\mu}$ instead of $\tilde{\nu}$, taking advantage of the flexibility in placing ρ inside or outside various derivatives. This is consistent with the spirit in which the model was devised. To this date, efforts to devise a curvature term with the required invariance properties and no d-dependence have failed. Note that curvature effects have been observed in free shear flows. Three-dimensional effects in boundary layers (i.e., pressure-gradient vector at an angle to the ve-

locity vector) are also delicate to introduce even empirically without violating the invariance principles. No plans have been made to depart from a scalar eddy viscosity.

Acknowledgements

The initial work was performed by the first author while an employee of NASA Ames Research Center. Dr. L. Wigton reviewed the manuscript and ran some of the cases. Mr. W. F. Nouss reviewed the manuscript. Ms. W. Wilkinson provided some of the files. We have benefited from comments by Drs. Baldwin, Barth, Birch, Bradshaw, Jou, Menter, Speziale, and Vandromme. These comments do not constitute endorsements.

Appendix: Summary of the Model. Version I

We solve the Reynolds-averaged Navier-Stokes equations and a transport equation for the turbulence model. The Reynolds stresses are given by $-\overline{u_i u_j} = 2\nu_t S_{ij}$ where $S_{ij} \equiv (\partial U_i/\partial x_j + \partial U_j/\partial x_i)/2$. The eddy viscosity ν_t is given by

$$\nu_t = \tilde{\nu}\, f_{v1}, \qquad f_{v1} = \frac{\chi^3}{\chi^3 + c_{v1}^3}, \qquad \chi \equiv \frac{\tilde{\nu}}{\nu}. \qquad (A1)$$

ν is the molecular viscosity. $\tilde{\nu}$ is the working variable and obeys the transport equation

$$\frac{D\tilde{\nu}}{Dt} = c_{b1}\,[1 - f_{t2}]\,\tilde{S}\,\tilde{\nu} + \frac{1}{\sigma}\left[\nabla\cdot((\nu+\tilde{\nu})\nabla\tilde{\nu}) + c_{b2}\,(\nabla\tilde{\nu})^2\right]$$
$$- \left[c_{w1} f_w - \frac{c_{b1}}{\kappa^2} f_{t2}\right]\left[\frac{\tilde{\nu}}{d}\right]^2 + f_{t1}\,\Delta U^2 \qquad (A2)$$

Here S is the magnitude of the vorticity,

$$\tilde{S} \equiv S + \frac{\tilde{\nu}}{\kappa^2 d^2} f_{v2}, \qquad f_{v2} = 1 - \frac{\chi}{1 + \chi f_{v1}}, \qquad (A3)$$

and d is the distance to the closest wall.

The function f_w is

$$f_w = g\left[\frac{1 + c_{w3}^6}{g^6 + c_{w3}^6}\right]^{1/6}, \qquad g = r + c_{w2}\,(r^6 - r), \quad r \equiv \frac{\tilde{\nu}}{\tilde{S}\kappa^2 d^2}. \qquad (A4)$$

For large r f_w reaches a constant, so large values of r can be truncated to 10 or so.

The wall boundary condition is $\tilde{\nu} = 0$. In the freestream 0 is best, provided numerical errors do not push $\tilde{\nu}$ to negative values near the edge of the boundary layer (the exact solution can't go negative). Values below $\nu/10$ will be acceptable. The same applies to the initial condition. The f_{t2} function is

$$f_{t2} = c_{t3}\, \exp(-c_{t4}\, \chi^2). \qquad (A5)$$

The trip function f_{t1} is as follows: d_t is the distance from the field point to the trip, which is on a wall. ω_t is the wall vorticity at the trip, and ΔU is the difference between the velocity at the field point and that at the trip. Then $g_t \equiv \min(0.1, \Delta U/\omega_t \Delta x)$ where Δx is the grid spacing along the wall at the trip, and

$$f_{t1} = c_{t1}\, g_t\, \exp\left(-c_{t2}\, \frac{\omega_t^2}{\Delta U^2}\,[d^2 + g_t^2 d_t^2]\right). \qquad (A6)$$

The constants are $c_{b1} = 0.1355$, $\sigma = 2/3$, $c_{b2} = 0.622$, $\kappa = 0.41$, $c_{w1} = c_{b1}/\kappa^2 + (1 + c_{b2})/\sigma$, $c_{w2} = 0.3$, $c_{w3} = 2$, $c_{v1} = 7.1$, $c_{t1} = 1$, $c_{t2} = 2$, $c_{t3} = 1.1$, $c_{t4} = 2$. Turbulent heat transfer obeys a turbulent Prandtl number (not to be confused with σ) equal to 0.9.

References

[1] Baldwin, B. S., & Lomax, H., "Thin layer approximation and algebraic model for separated turbulent flows", AIAA-78-257.

[2] Cebeci, T., & Smith, A. M. O.,"A finite-difference method for calculating compressible laminar and turbulent boundary layers", Journal of Basic Engineering, Vol. 92, No. 3, pp. 523-535.

[3] Johnson, D. A., & King, L. S., "A mathematically simple turbulence closure model for attached and separated turbulent boundary layers", AIAA Journal, Vol. 23, No. 11, 1985, pp. 1684-1692.

[4] Mavriplis, D. J., "Algebraic Turbulence Modeling for Unstructured and Adaptive Meshes", AIAA-90-1653.

[5] Launder, B. E., & Tselepidakis, D. P., "Directions in second-moment modelling of near-wall turbulence", AIAA-91-0219.

[6] Holst, T. L., "Viscous transonic airfoil workshop. Compendium of results", AIAA-87-1460.

[7] Viegas, J. R., Rubesin, M. W., & Horstman, C. C., "On the use of wall functions as boundary conditions for two-dimensional separated compressible flows", AIAA-85-0180.

[8] Baldwin, B. S., & Barth, T. J., "A one-equation turbulence transport model for high Reynolds number wall-bounded flows", AIAA-91-0610.

[9] Bradshaw, P., Ferriss, D. H., & Atwell, N. P., "Calculation of boundary-layer development using the turbulent energy equation", J. Fluid Mech., Vol. 28, 3, 1967, pp. 593-616.

[10] Nee, V. W., & Kovasznay, L. S. G., "Simple phenomenological theory of turbulent shear flows", Physics of Fluids, Vol. 12, No. 3, 1969, pp. 473-484.

[11] Secundov, Smirnova, Kozlov, & Gulyaev. "One-equation eddy viscosity model (modified L. S. J. Kovasznay model)". Short summary of the equations. Personal communication, 1990.

[12] Mitcheltree, R. A., Salas, M. D., & Hassan, H. A., "One-equation turbulence model for transonic airfoil flows", AIAA Journal, Vol. 28, No. 9, 1990, pp. 1625-1632.

[13] Bradshaw, P., Launder, B. E., & Lumley, J. L., "Collaborative testing of turbulence models", AIAA-91-0215.

[14] Wilcox, D. C., "Reassessment of the scale-determining equation for advanced turbulence models", AIAA Journal, Vol. 26, No. 11, 1988, pp. 1299-1310.

[15] Spalart, P. R., "Direct simulation of a turbulent boundary layer up to $R_\theta = 1410$", J. Fluid Mech., Vol. 187, 1988, pp. 61-98.

[16] Baldwin, B. S., & Barth, T. J., "A one-equation turbulence transport model for high Reynolds number wall-bounded flows", NASA TM 102847, 1990.

[17] Townsend, A. A. The structure of turbulent shear flow. Cambridge University Press, New York, 1976.

[18] Schlichting, H. Boundary-layer theory. McGraw-Hill, New York, 1979.

[19] Hunt, J. C. R. "Turbulence structure in thermal convection and shear-free boundary layers". J. Fluid Mech., Vol. 138, 1984, pp. 161-184.

[20] Mellor, G. L., & Herring, H. J., "Two methods of calculating turbulent boundary layer behavior based on numerical solution of the equations of motion". Proc. Conf. Turb. Boundary Layer Pred., Stanford, 1968.

[21] Martinelli, L., & Jameson, A., "Validation of a Multigrid Method for the Reynolds Averaged Equations", AIAA-88-0414.

[22] Steinthorsson, E., & Shih, T. I.-P., "A Method of Reducing Approximate Factorization Errors in Two- and Three-Factored Schemes", submitted to SIAM J. of Statistical and Scientific Computing.

[23] Shih, T. I.-P., & Chyu, W. J., "Approximate Factorization with Source Terms", AIAA Journal, Vol. 29, No. 10, October 1991, pp. 1759-1760.

[24] Samuel, A. E., & Joubert, P. N. "A boundary layer developing in an increasingly adverse pressure gradient", J. Fluid Mech., Vol. 66, 3, 1974, pp. 481-505.

[25] Menter, F. R., "Performance of popular turbulence models for attached and separated adverse pressure gradient flows", AIAA-91-1784.

[26] Cook, P. H., McDonald, M. A., & Firmin, M. C. P., "Aerofoil RAE 2822 – Pressure distributions, and boundary layer and wake measurements", AGARD-AR-138, 1979.

[27] Swanson, R. C., & Turkel, E., "Artificial Dissipation and Central Difference Schemes for the Euler and Navier-Stokes Equations", AIAA-87-1107, 1987.

[28] Wigton, L. B., "High Quality Grid Generation Using Laplacian Sweeps", Fourth International Symposium on Computational Fluid Dynamics, U.C. Davis, Sep. 1991, pp. 1222-1228.

[29] Cook, P. H., & McDonald, M. A., "Wind tunnel measurements in the boundary layer and wake of an airfoil with a blunt base at high subsonic speeds", RAE Tech. Rept. 84002, 1984.

[30] Henne, P. A., & Gregg, R. D., "A new airfoil design concept", AIAA-89-2201-CP.

[31] Drela, M., "Integral boundary layer formulation for blunt trailing edges", AIAA-89-2200.